ISAS - INTERNATIONAL SCHOOL
FOR ADVANCED STUDIES

BIOPHYSICS OF THE COCHLEA. THEORY, EXPERIMENTS AND APPLICATIONS

Thesis submitted to the
International School for Advanced Studies, Trieste, Italy
- *Biophysics Sector* -
in partial fulfillment of the requirements for the degree of

Doctor Philosophiae

Candidate:
Fabio Mammano

Supervisor:
Dr. Jonathan F. Ashmore

Academic Year 1990/1991

SISSA - SCUOLA
INTERNAZIONALE
SUPERIORE
DI STUDI AVANZATI
TRIESTE
Strada Costiera 11

TRIESTE

BIOPHYSICS OF THE COCHLEA. THEORY, EXPERIMENTS AND APPLICATIONS

Thesis submitted to the
International School for Advanced Studies, Trieste, Italy
- *Biophysics Sector* -
in partial fulfillment of the requirements for the degree of

Doctor Philosophiae

Candidate:
Fabio Mammano

Supervisor:
Dr. Jonathan F. Ashmore

Academic Year 1990/1991

Abstract

This work attempts to bring together theoretical and experimental aspects of cochlear biophysics. In both cases, the focus is on the relationship between the motility of outer hair cells and the filtering properties of the basilar membrane, as this seems the key for understanding the functioning of the peripheral auditory system.

From the theoretical side, the hydrodynamics of the cochlea is studied in detail. A possible mechanism for coupling the outer hair cells to the mechanics of the basilar membrane is proposed and analysed mathematically. From the experimental side, the effects of stimulating the cochlea with extracellular current are investigated by means of laser interferometry. The necessary apparatus and the software for data acquisition were engineered in the course of this investigation. A rapid return in the realm of mathematical modelling concludes this work, with an eye on possible applications of physiological knowledge to speech recognition.

The newcomer is given a succint introduction to the cochlear world in Chapter 1. A new model of cochlear biomechanics is presented in Chapter 2. A set of experiments aiming at clarifying the role of outer hair cell motility in the control of the vibration pattern of the basilar membrane are described in Chapter 3. The role of active cochlear mechanics in the processing of speech is explored in Chapter 4. Chapters 2 and 4 are the result of an intense collaboration with Prof. Renato Nobili at the Department of Physics of Padova University, Italy, following a preparatory period with Prof. Campbell L. Searle at the Massachusetts Institute of Technology, Boston, U.S.A. The results of Chapter 3 were obtained thanks to the expertise of Dr. Jonathan Ashmore, in his laboratory at the Department of Physiology of Bristol University, England.

Aknowledgments

I am grateful to Prof. Renato Nobili for his enthusiastic involvement in the development of our model and to Dr. Jonathan F. Ashmore for teaching that theoreticians use their minds whereas experimentalists use their hands too.

I am indebted to Prof. Campbell L. Searle for offering me the opportunity to study in M.I.T, to Prof. Andrea Donato for his interest in the mathematical aspects of this work, to Dr. Paul Kolston for his criticism and to Jonathan Gale for helpful discussions and amusement in Bristol.

I enjoyed Dr. Oscar Moran's help during my initiation to the experimental world.

This thesis was financially supported by a Postgraduate Scholarship from the International School for Advanced Studies in Trieste, Italy.

Contents

Chapter 1

Introduction

1.1 Overview of cochlear morphology and function

The inner ear is a set of extremely delicate organs buried, in humans, in the hardest bone in the body, the *petrous temporal bone*. It comprises the organs of equilibrium and of hearing. Because of its shape, the organ of hearing is called *cochlea* (Latin for "snail shell", Fig.1.1a). Internally, it consists of three parallel canals coiled together and spiralling around the *modiolus*. This is a double–threaded screw–shaped bony structure forming the central support of the cochlea. The cochlear canals are named *scala vestibuli, scala media* and *scala tympani*. Scala vestibuli is separated from scala media by a thin deformable sheet, called *Reissner's membrane* (RM). Scala media is separated from scala tympani by a more resistant structure, the *basilar membrane* (BM), upon which a thickened ridge, the *organ of Corti*, runs along. Scala tympani and scala vestibuli, which communicate with one another at the *helicotrema* hole (H), are filled with *perilymph*, a fluid rich in Na^+ (ca. 140 mmol/l). The scala media is filled with *endolymph*, rich in K^+ (ca. 155 mmol/l). The difference in ion composition of the two media is responsible for the potential difference of about + 80 mV normally measured between the endolymphatic and the perilymphatic space. From a purely hydromechanical standpoint the presence of the RM, comoving with the fluid, can be totally neglected and therefore SV and

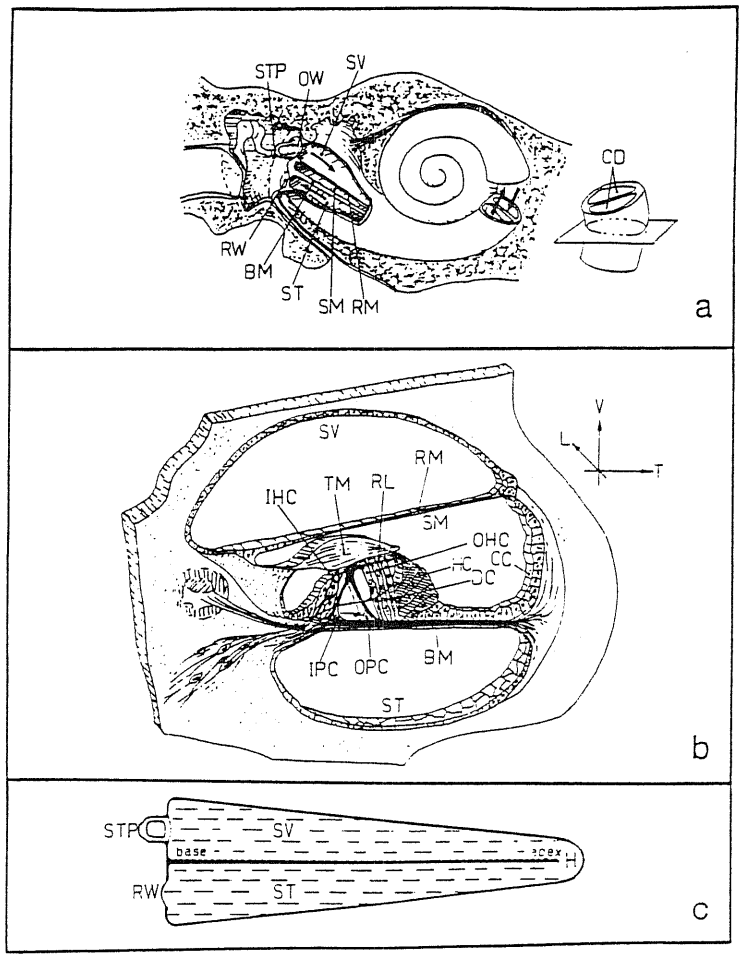

Figure 1.1: Longitudinal (a, c) and transversal (b) sections of a cochlea, showing stapes (ST), basilar membrane (BM), helicotrema hole (H), inner and outer pillar cells (IPC, OPC), inner and outer hair cells (IHC, OHC), Hensen's cells (HC), Claudius' cells (CC), reticular lamina (RL), tectorial membrane (TM), scala tympani (ST), scala vestibuli (SV), cochlear duct (CD). At the oval window (OW), the stapes footplate adjoins the perilymph of the scala vestibuli. The opening is sealed off by the *annular ligament* (not shown), so that no perilymph can leak out. At the base of scala tympani is another opening to the middle ear, the round window (RW), sealed by a fine membrane to prevent leakage of perilymph.

SM can be identified as one compartment.

For the sake of clarity, let us define the local orientation of a cochlear section as follows: the plane of the BM is regarded as horizontal, hence the BM displacements under sound stimuli are regarded as *vertical* (V). The local direction from base to apex is defined as *longitudinal* (L) and the direction parallel to the BM fibres, radially oriented towards the external side of the cochlea, as *transversal* (T). Then, for instance, Fig.1.1b shows a transversal section of the cochlea, whereas Fig.1.1c shows a longitudinal section of an ideally uncoiled cochlea.

The BM is a system of parallel elastic fibres, each formed by hundreds of protein filaments, tensed between the internal bony prominence of the cochlear duct and embedded in a cottony ground substance (Iurato, 1962; Cabezudo, 1978). The auditory organ appears as a tapered elastic structure which spirals out from the helicotrema side the (*apex*) to the stapes side the (*base*), gradually decreasing in thickness and increasing in width. As the BM is transversally tensed all along the cochlear duct, this structure is elastically sensitive to the pressure differences between its opposite faces, which are ultimately proportional to local fluid acceleration differences caused by acoustical excitation.

The organ of Corti contains specialized receptors, responsible for auditory function, that are firmly embedded in a relatively rigid structure (Fig.1.1b). Such receptors are called *hair cells* because they possess bundles of thin stiff tubules called *stereocilia*, which are located at their apical surface and are grouped in multiple arrays linked together by protein filaments (Pickles, 1988). The *inner* hair cells (IHCs; about 3,500 in humans) run along the BM in a single row whereas the *outer* hair cells (OHCs) run in triplets (about 4,000 triplets in humans). The IHCs have sack–shaped unmotile cell bodies located in the proximity of the osseous spiral prominence, where the basilar membrane motion is expected to be minimal; the OHCs have cylindrical motile cell–bodies ending at the apical region in a rigid platform called the *cuticular plate*, where the stereocilia are inserted.

The afferent nerve fibres innervating the hair cells come from the bipolar neurons of the *spiral ganglion*, which lies at the centre of the cochlea. The axons of these cells run to the central nervous system. About 90% of the spiral ganglion neurons have

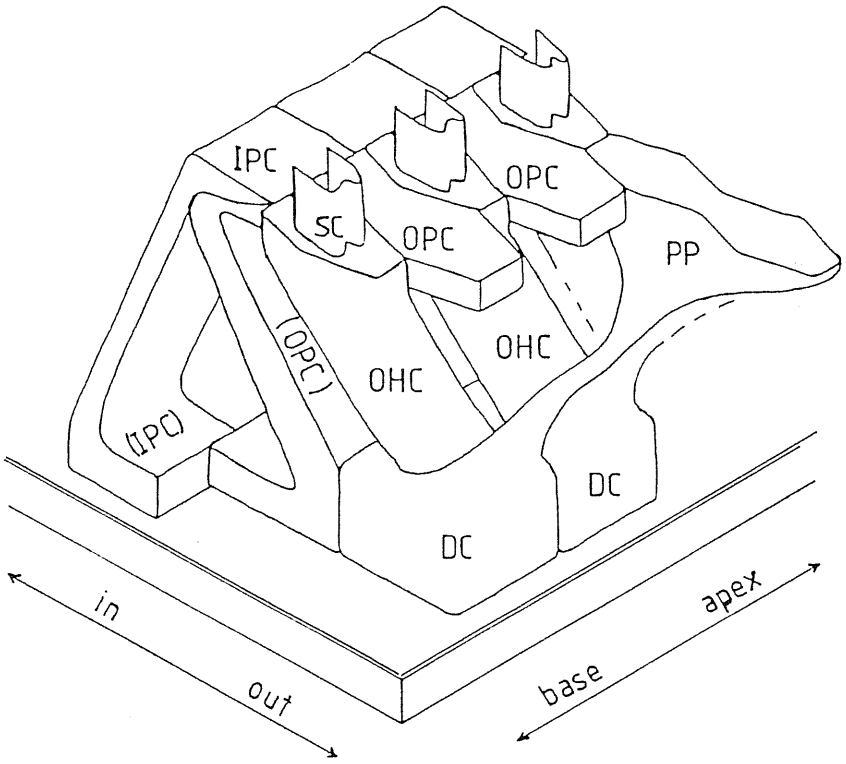

Figure 1.2: The ultrastructure of the organ of Corti. Stiff components: inner pillar cells (IPC), outer pillar cells (OPC), Dieters' cells (DC), phalangeal processes of the DCs (PP). The OHCs are firmly held at their basal region by the cup–shaped bodies of DCs. Apically, they end in stiff hexagonal plates, tightly connected to the stiff edges of the funnel–shaped ends of PPs. All these elements form the reticular lamina (RL), which is rather stiff under torques around longitudinal axes but more compliant under longitudinal deformations.

endings innervating the IHCs and each of these, in turn, makes contact with several nerve fibres. Only the remaining 10% of fibres innervate the far more numerous OHCs. Altogether, the auditory nerve contains 30,000 to 40,000 afferent fibres. The organ of Corti also receives efferent fibres. Most of these project inhibitory synapses onto the OHC bases and are thought to control the activity of these cells (Spoendlin, 1978; Kim, 1984).

The structure embedding the hair cells is formed by supporting cells, all having very similar stiff cytoskeletal organization, differing from each other mainly in their shape: *inner pillar cells* (IPCs), *outer pillar cells* (OPCs), *Dieters' cells* (DCs) (Iurato, 1961; Lim, 1986). Adjacent to this structure, there are the Hensen's cells

which delimits the space where the OHCs are hosted. Beyond this, there is the layer of Claudius' cells covering the BM from the Hensen's cell region up to the external bony prominence of the cochlear duct. The lower parts of all these cells are fixed to the BM. The shape of the DCs is determined by the peculiar way they are connected to both the basal and the apical ends of the OHCs, i.e. by their cup–shaped basal part and the phalangeal process, respectively (Fig.1.2). The phalangeal processes branches out from the DC body, turning away from the enveloped OHC towards the cochlear apex. Then, skipping the adjacent OHC triplet, the process ends at the level of the OHC cuticular plate, where it expands in a squashed–funnel–shaped portion with a bihexagonal contour. The IPCs and OPCs are tightly connected at their upper portions and form a triangular structure opened wide apart onto the BM. The lower parts of OPCs are not aligned with those of the IPCs, joined to them at the upper sides, along the direction of the BM fibres, but are shifted towards the opposite direction with respect to the DC phalanges, i.e. towards the cochlear base (L. Voldřich, 1983). The joined upper portions of the pillar cells form an arch–shaped prominence extending to the cuticular plate of the 1st series of OHCs. This arch possesses peripheral thickenings which, joined together and to the thickenings contouring the OHC cuticular plates and the ends of Dieters' cell phalanges, are closely tiled to form the so called *reticular lamina* (RL). This is paved according to a hexagonal symmetry. Because of its peculiar morphology, characterized by a systematic thickening of the cell junctions in the transversal direction and by the contour deformability of the phalangeal processes in the longitudinal direction, *the RL is expected to be rather stiff under bending around longitudinal axes, but more compliant under longitudinal stretching or compression.*

Over the organ of Corti lies the *tectorial membrane* (TM), a gelatinous mass embedding a system of transversal fibres (Steel, 1986), attached to the modiolar side of the cochlear duct and to the organ of Corti (Fig.1.1b). The TM is separated from the RL by a narrow fluid–filled space. The stereocilia of the IHCs contact the TM at the level of the *Hensen's stripe* but probably do not adhere to it (Lim, 1986). The W-shaped bundles of stereocilia of the OHCs span the subtectorial gap and are partially fixed into the underside of the TM. When such a bundle is pushed in the direction of its symmetry axis, stereocilia pivot about their insertion point into

the cuticular plate. A remarkable feature of the OHC bundles is their considerable pivotal stiffness. Richardson *et al.* (1989) estimated the stiffness presented by the central fraction of the stereocilia bundle of a single OHC (from the base of the cochlea) to be not less than 3×10^{-3}N/m, for displacements in the aforementioned direction. The pivotal stiffness of the bundle as a whole can be estimated by multiplying this figure by about 30–40 (there are about 100 stereocilia in a bundle), or possibly by more than that if the particular geometry of the bundle is considered (de Boer, 1991). This implies that the order of magnitude of the comprehensive stereocilia stiffness of an OHC triplet is likely to be larger than 0.1 N/m. In the next chapter we will discuss a functional reason for such a large values of the stiffness.

When the stapes is set into oscillation by acoustical excitations coming from the auditory meatus, sound energy is transmitted to the perilymph in the scala vestibuli. Because of fluid incompressibility, there must be some structure permitting fluid motion. This structure is the *round window* (RW), the membrane of which moves out as the stapes moves in, and vice versa. At the same time, the movements of the stapes causes the BM to swing up and down. Because of the rigidity of the pillar cell–reticular lamina framework, this motion is converted into a shear displacement of the RL relative to the TM, which deflects the hair cell cilia either by direct contact with the TM (for OHCs) or possibly by viscous drag (for IHCs). The pivoting of the stereocilia bundles in the outgoing radial direction causes the depolarization of the IHCs, which induces spike discharges in the contacting afferent nerve endings (Davis, 1958). The analogous stimulation of OHCs induces contraction of these cells through depolarization and, consequently, a mechanical reaction of the organ of Corti. Because of the stereocilia–bundle stiffness, the TM is forced to follow the RL motion with some degree of shearing with respect to it. So, the deflection of the stereocilia is also affected by the inertial reaction of the TM.

1.2 The quest for the cochlear amplifier

More than one century ago, it was realized that the frequency analysis performed by the cochlea depends upon the remarkable ultrastructure of the BM. In humans,

the thickness of the BM decreases about ten–fold while its width increases about five–fold from base to apex (Wever, 1938). Helmholtz (1863) assumed that the transversal portions of the BM act as local resonators, each one tuned at a different frequency. Tuning was supposed to vary continuously along the BM so that the stimulation by a particular tone would set into vibration only a small group of resonators in one region. The BM should be deflected principally in this region, and only there the nerve fibres should be excited.

Indirect measurements of the BM fibre stiffness in cochleas from cadavers (von Békésy, 1960) and direct measurements in fresh preparations (Gummer *et al.*, 1981) showed that the stiffness decreases by several orders of magnitude from base to apex (five in humans and as much as six in the guinea–pig), seemingly in agreement with Helmholtz's suggestion. Unfortunately, the physical behaviour of the cochlear system is not so simple, because the BM is immersed in the cochlear fluid. By its hydrodynamic action, the perilymph provides not only the coupling of the BM to the sound source via stapes motion, *but also the instantaneous intercoupling among all of the oscillating parts of the BM.* As firstly stressed by von Békésy (1960), precisely this hydrodynamic coupling is principally responsible for the characteristic responses of the organ of Corti to sounds. In the absence of OHC activity, the BM response to a sinusoidal perturbation at the stapes is a broad wave–like deflection with phase delay augmenting from base to apex, called *travelling wave* (TW) by von Békésy. For a tone of any given frequency, the vibration of the BM increases in amplitude as the wave travels towards the helicotrema. The wave then dies out rapidly beyond a certain site which depends upon the sound frequency in a characteristic way. Low–frequency sounds peak a long way along the BM, near the apex, and high–frequency sounds peak near the base. In this way, a coarse frequency–to–position logarithmic mapping is realized.

The gross profile of the TWs described by von Békésy (Fig.1.3a) largely contrasts with the sharp frequency selectivity of the mammalian auditory system seen in neural recordings. Von Békésy's observations were performed on the cochleas of cadavers at extremely loud intensities, greater than 100 dB *sound pressure level* (SPL). It is now known that the cochlea must be in excellent physiological condition in order for the BM to show a degree of tuning comparable to that displayed

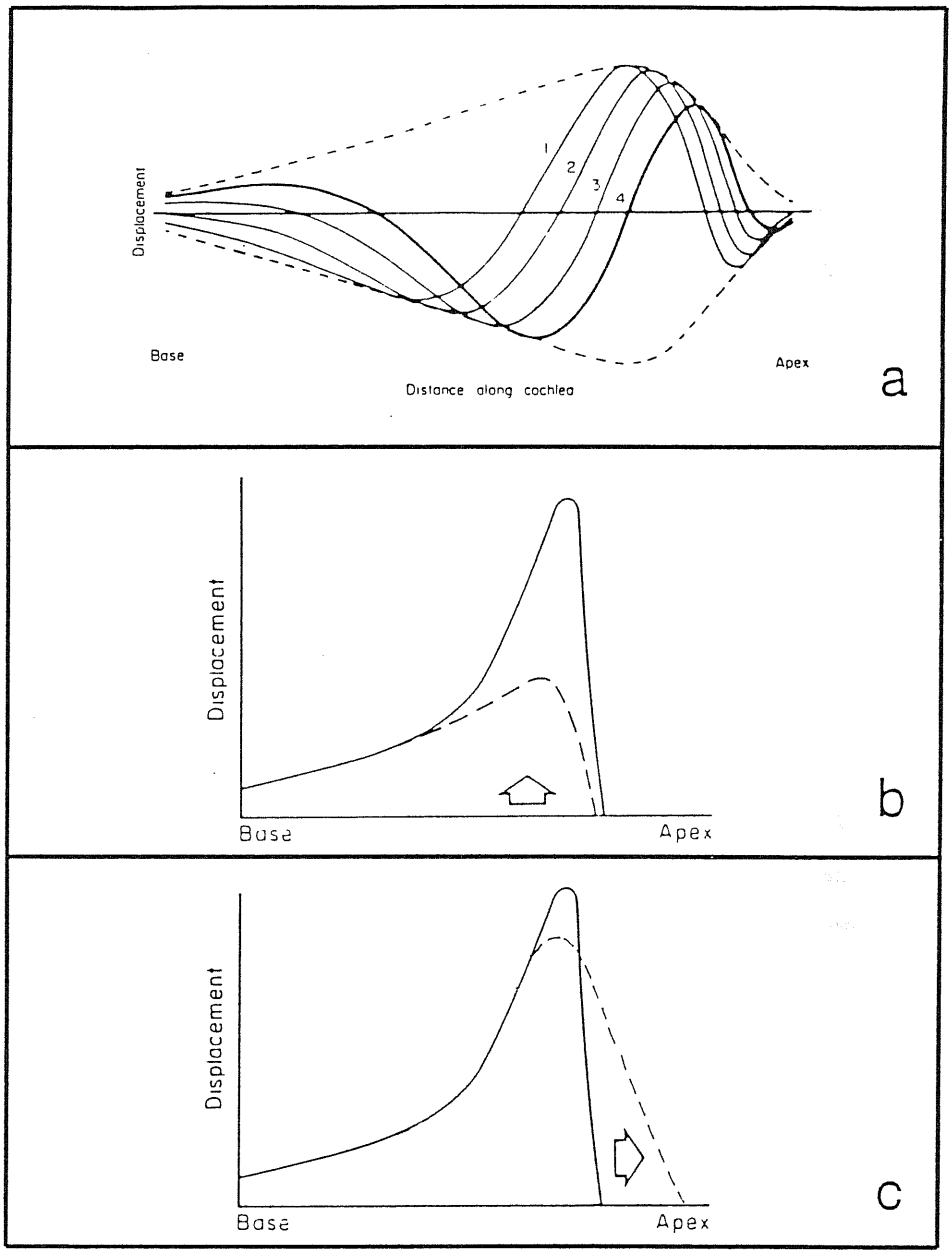

Figure 1.3: Travelling waves as observed (a) in cochleas from cadavers (von Békésy, 1960); b) in living animals, as inferred from fixed–point amplitude responses (from Pickles, 1988). c) Longitudinal coupling terms due to both bending and stretching reactions of the organ of Corti structure affect the slope of the TW as qualitatively represented by the dashed lines.

by neural data (Sellick *et al.*, 1982; Robles *et al.*, 1986). Moreover, the experimental results of the last decade, obtained by both Mössbauer techniques and by laser interferometry, all agree in that the tuning of the BM is SPL–dependent. It is extremely sharp at low SPLs (where it matches perfectly the tuning of neural recordings) and broadens as the stimulus amplitude is increased above the auditory threshold. The sharp mechanical tuning (Fig.1.3b) depends on a *physiologically vulnerable* mechanism located inside the organ of Corti (Johnstone *et al.*, 1986; Pickles, 1988; Dallos, 1988), generally referred to as the *cochlear amplifier.*

Long before the discovery of OHC motility, the need for a cochlear amplifier was suspected by Gold (1948). Yet, for a long time it was not understood why the vast majority of the auditory afferents receive inputs from the IHCs, whereas OHC afferent innervation is scarce. The function of the far more numerous OHCs was unexplained. The two problems have not been related to each other until recently. As shown by Kiang *et al.* (1970), in cats injected with aminoglycoside antibiotics, which are now known to damage OHCs, the sharply–tuned low–threshold tip of the neural tuning curves are selectively raised, while the low–frequency tail is unaffected. These findings are confirmed by mechanical measurements of the BM responses under the effect of furosemide (Ruggero and Rich, 1991), which is supposed to affect the OHCs more than the IHCs by reducing the potential difference between endolymph and perilymph.

Ashmore (1987) demonstrated that OHCs contract when depolarized and elongate when hyperpolarized under voltage clamp conditions *in vitro.* These motile responses associated with membrane potential changes are now called into question in order to account for the existence of the cochlear amplifier. As documented by de Boer (1991), three main ways have been so far conceived (see for instance: 1. Neely and Kim, 1986; 2. Zwicker, 1986; 3. Kolston, 1988) to explain how sharp frequency selectivity may be achieved in the functioning cochlea. All of them require active processes for energy supply, conceivably by the action of OHCs. Yet, none of them consider the severe limitations imposed by OHC physiology. The aforementioned approaches are invariably cast in the framework of transmission–line models, which are unlikely to reliably describe the cochlear dynamics, since the long–range character of hydrodynamical interactions is completely neglected. A more reliable

hydromechanical analysis of the cochlea, as a merely physical system, is presented in the following chapter.

Chapter 2

Biophysics of the cochlea

2.1 Abstract

A novel analysis of the cochlear function limited to the linear approximation is presented, paying attention to the constraints imposed by recent findings of cochlear anatomy and physiology. The law of motion of the basilar membrane in the absence of active processes is derived in the form of an integral equation. The hydro–mechanical properties of the cochlear partition are expressed in the form an integral kernel. Solutions of the equation are obtained by inversion of the kernel. The motion equation for the active cochlea is then derived, assuming that the motility of outer hair cells provides a pseudo–elastic contribution to the stiffness of the basilar membrane. The low–pass–filter characteristics of the hair cell membrane are included. The enhancement of the hair–cell triggering–sensitivity at high frequencies, which is required for the cochlear activity to be undamped all over the acoustical frequency range, is explained by the intervention of inertial effects of the tectorial membrane. Numerical simulations of the responses of the basilar–membrane to pure tones are presented. In the absence of active processes, the formation of travelling waves, as observed in post–mortem specimens, is evidenced. When the action of the outer hair cells is included, sharply tuned responses are obtained. Both magnitude and phases of the simulated responses agree with experimental data.

2.2 The mechanical structure of the cochlea

The organ of Corti is a modular structure formed by a long array of adjacent substructures, each hosting a triplet of outer hair cells (OHCs). In the following, these substructures will be referred to as *segments*. At first glance, such segments may seem freely moving with respect to each other with negligible viscoelastic strengths in between, so that, mechanically, the basilar membrane (BM) would be equivalent to a collection of independent parts intercoupled only by the surrounding fluid. Several models include this simplifying assumption, without justification.

As it was already noticed by de Boer (1984) – longitudinal couplings like those taking place in an elastic string or in a beam, respectively represented by terms proportional to space derivatives up to the second or to the fourth order, would affect the BM behaviour precisely in the opposite way with respect to what seems desirable for a good model and furthermore is known from experiments. Such terms would affect the shape of the travelling wave (TW) so as to decrease the slope of descent of the amplitude envelope towards the apex (as approximately shown by the dashed lines in Fig.1.3c).

On the other hand, although the elastic fibres tensing the BM are not appreciably intercoupled, the vertical displacements of the BM segments (or, more exactly, the local deformations of the cochlear partition) seem to affect each other in complex manners: internally, by the sophisticated interdigitation of the supporting cells; on the upper side, by the asymmetric stiffness of the reticular lamina (RL). The RL must be regarded as a thin albeit stiff plate, longitudinally weakened by the hollow squashed–funnel structure of the Dieters' cell phalangeal expansions, rather than as a simple array of adjacent but disjointed segments or as an elastic membrane. As it has already been stressed in the previous section, the RL is likely to be considerably stiffer with respect to transversal than to longitudinal deformations. Unfortunately, besides the beautiful detailed images provided by electronic microscopy (Angelborg and Engstrom, 1973; Harada, 1983; Slepecky and Chamberlain, 1987), direct knowledge of the mechanical interplay amongst the supporting elements of the organ of Corti is not yet available. These estimates were derived indirectly, by structural and functional considerations and are only qualitative. We determined the main

characteristics of the passive cochlear dynamics by collecting together these incomplete pieces of information from specialized literature, as briefly described in the remainder of this section.

In the cochlea of living animals, differences in sound–induced vertical displacements of the BM are appreciable only over distances covering more than three or four OHC triplets. This corresponds to the width of the best–tuned responses to tonal stimuli at the peak of the response. As the waveforms of the passive cochlea are by far smoother than the best–tuned responses, the displacement of the BM segments can be represented in any case by a continuous variable and the dynamical laws governing the BM motion can be described in the framework of the integro–differential formalism. The longitudinal coordinate of the BM can be represented by the continuous variable x spanning the interval [0, 1] with the extremes corresponding to base and apex, respectively. The vertical displacement of the BM at point x and time t will be indicated by $\xi(x,t)$. Upperdots over time–depending variables will represent partial derivatives after t. The law governing the motion of the cochlea, in the absence of active processes, is obtained by equating to zero the algebraic sum of the forces acting at any given time t on a BM segment of infinitesimal length centered at x. The largest oscillation amplitudes of the BM found in normal conditions are very small (tenths of a μm; Sellick *et al*, 1982). Furthemore, both the velocity field of fluid and its gradient keep very small. Hence, the linear approximation is perfectly justified as long as no active process is involved. We assume that all the force terms depend linearly on the displacements of the cochlear segments and on their time derivatives. These terms are:

• The *mechanical inertial* term accounting for the local inertial reaction of the organ of Corti:

$$-\,m(x)\,\ddot{\xi}(x,t)\,, \tag{2.1}$$

where $m(x)$ is the mass per unit length of the cochlear partition. Since the thickness of the organ of Corti is approximately the same all along its length, we assume that $m(x)$ is proportional to the BM width $b(x) \approx 0.12 \times \exp(1.28x)$ mm, after Wever (1938).

- The *fluid viscosity* term:

$$h(x)\,\dot{\xi}(x,t)\,,$$

where coefficient $h(x)$ accounts for all kinds of viscosity affecting the absolute vertical motion of the organ of Corti. We will return on this at the end of the section. In what concerns the dissipative effects of the perilymph, a simple dimensional computation shows that, excluding the case of sound excitations of abnormal amplitudes, the Reynolds' numbers associated with the motions of the different parts of the cochlear system remain below 30–40. Consequently, the fluid dynamics is simply affected by viscous forces in a laminar regime. Among these forces, the resistance due to the fluid shear within the narrow RL–TM cleft (1–5μm) is overwhelming, although it is limited by the stereocilia elastic reaction. In the following, this term will be referred to as *TM cleft resistance*. This suggests that $h(x)$ is proportional to the transversal width and inversely proportional to the height of the RL–TM cleft. Both these quantities vary little along the cochlea. Hence, assuming that

$$h(x) \propto \exp(-\alpha\, x)$$

a small value for the exponent is expected. We return on this in section 2.4. To neutralize the dissipative effects of this viscosity term, a counterterm locally proportional to the vertical velocity of the BM is needed for an active cochlea. We deal with this in section 2.5.

- The *fibre stiffness* term:

$$k(x)\,\xi(x,t)\,,$$

where $k(x)$ is the elastic constant of the BM with respect to its vertical displacement at x. Note that $k(x)$ would be zero if the BM fibres were not tensed. In principle, its magnitude might depend on the state of tension of the BM, i.e. on $\xi(x,t)$ itself. Of course, this would affect the BM mechanics in a non–linear way. But we need not worry about this because: a) in normal conditions, the BM fibres are in tension; b) the experimental diagrams of the BM stiffness vs. vertical displacement exhibit plateaux, at values not exceeding 0.2 N/m per cochlear segment (at the base), within wide intervals of the argument (Gummer *et al.*, 1981; Miller, 1985; Olson and Mountain, 1991). We assume $k(x) \propto \exp(-\beta\, x)$, where $\beta \approx 5$, in agreement with the experimental data (Gummer *et al.*, 1981; de Boer, 1981; de Boer 1984).

• The *longitudinal elastic* term, accounting for the longitudinal stretching stiffness of the RL:

$$g_e(x)\frac{\partial}{\partial x}f_e(x)\frac{\partial \xi(x,t)}{\partial x}\,,$$

where $g_e(x)$ is the longitudinal elastic coefficient of the RL at x and $f_e(x)$ is a form factor accounting for possible lack of homogeneity in the longitudinal direction. This term would be significant if the RL were longitudinally in tension. Since the RL structure, which is weakened by the hollows of the Dieters'–cell phalangeal processes, is longitudinally relaxed, this term is likely to be negligible.

• The *bending strength* term, arising from local torques of the organ of Corti around transversal axes:

$$g_b(x)\frac{\partial^2}{\partial x^2}f_b(x)\,\frac{\partial^2 \xi(x,t)}{\partial x^2}\,,$$

where $g_b(x)$ is the local bending coefficient and $f_b(x)$ accounts, as $f_s(x)$ did in the former case, for possible shape non–homogeneity. Since the organ of Corti is basically connected only by the transversally thin, albeit stiff, RL, this term is also expected to be negligible.

• The *shear viscosity* term arising from the mutual friction between adjacent segments:

$$g_s(x)\frac{\partial}{\partial x}f_s(x)\frac{\partial \dot{\xi}(x,t)}{\partial x}\,,$$

where $g_s(x)$ is the shear viscosity coefficient and $f_s(x)$ is a suitable form factor depending on possible longitudinal non–homogeneity of the system. Since the shear displacements between adjacent segments are prevented by the stiffness of the RL, we assume that this space–derivative term is also negligible.

• The *hydrodynamic stapedial force* term. It represents the force $F_S(x,t)$ caused by the stapes motion and transmitted by the fluid to a BM segment at x:

$$F_S(x,t) = -G_S(x)\,\ddot{\sigma}(t)\,, \tag{2.2}$$

where $\sigma(t)$ is the stapes displacement at time t. We called $G_S(x)$ the *hydrodynamic stapes propagator*, as it represents the force per unit length caused by the stapes acceleration $\ddot{\sigma}(t)$ and transmitted by the fluid pressure difference across the BM at point x.

• The *hydrodynamic inertial force* term. This is the force $F_{BM}(x,t)$ acting on a BM segment at x due to the motion of all the BM segments and transmitted by the fluid pressure. It is expressed as an integral:

$$F_{BM}(x,t) = -\int_0^1 G(x,\bar{x})\,\ddot{\xi}(\bar{x},t)\,d\bar{x}\,. \tag{2.3}$$

We called $G(x,\bar{x})\,d\bar{x}$ the *hydrodynamic propagator* at x, as it represents the pressure contribution due to the motion of the $d\bar{x}$–wide BM segment at $\bar{x}$. Assuming the validity of the linear approximation, this term is proportional to the local acceleration of the BM and is by far the most important coupling term the dynamics of the cochlear partition. Accurate descriptions of the propagators $G_S(x)$ and $G(x,\bar{x})$ are given in the following section.

2.3 The hydrodynamic propagators

The hydrodynamic force terms $F_S(x,t)$ and $F_{BM}(x,t)$, introduced in the previous section, are proportional to the pressure difference across a BM segment at x. They respectively summarize the actions of the stapes and of the whole BM simultaneously transmitted by the fluid. In the limit of small fluid–boundary displacements and velocities, the pressure field $p(\vec{r})$ of an incompressible fluid and the local fluid acceleration $\vec{a}(\vec{r},t) = \partial\vec{v}(\vec{r},t)/\partial t$ are linked by the equation

$$\vec{\nabla}p(\vec{r},t) + \rho\,\vec{a}(\vec{r},t) = 0\,. \tag{2.4}$$

where ρ is fluid density, $\vec{r}$ is the vector representing a point within the fluid, $\vec{v}(\vec{r},t)$ is the velocity field and $\vec{\nabla}$ is the gradient operator acting on $\vec{r}$. Under the assumed conditions the velocity field is irrotational and also solenoidal because of the fluid incompressibility. Therefore we can put $\vec{v}(\vec{r},t) = \vec{\nabla}\phi(\vec{r},t)$, where $\phi(\vec{r})$ is a scalar field, called the *kinetic potential* (see, for example, Tritton, 1977). Then Eq. (2.4) can be integrated all over the fluid yielding

$$p(\vec{r},t) + \rho\,\frac{\partial\phi(\vec{r},t)}{\partial t} = \text{const}\,, \tag{2.5}$$

$\phi(\vec{r},t)$ satisfies equation $\nabla^2\phi(\vec{r},t) = 0$ and the boundary conditions $\vec{\nabla}\phi(\vec{r}_b,t) = \vec{v}(\vec{r}_b,t)$ where $\vec{v}(\vec{r}_b,t)$ is the velocity of the cochlear fluid boundary at $\vec{r}_b$ (vanishing everywhere except at stapes and BM surfaces).

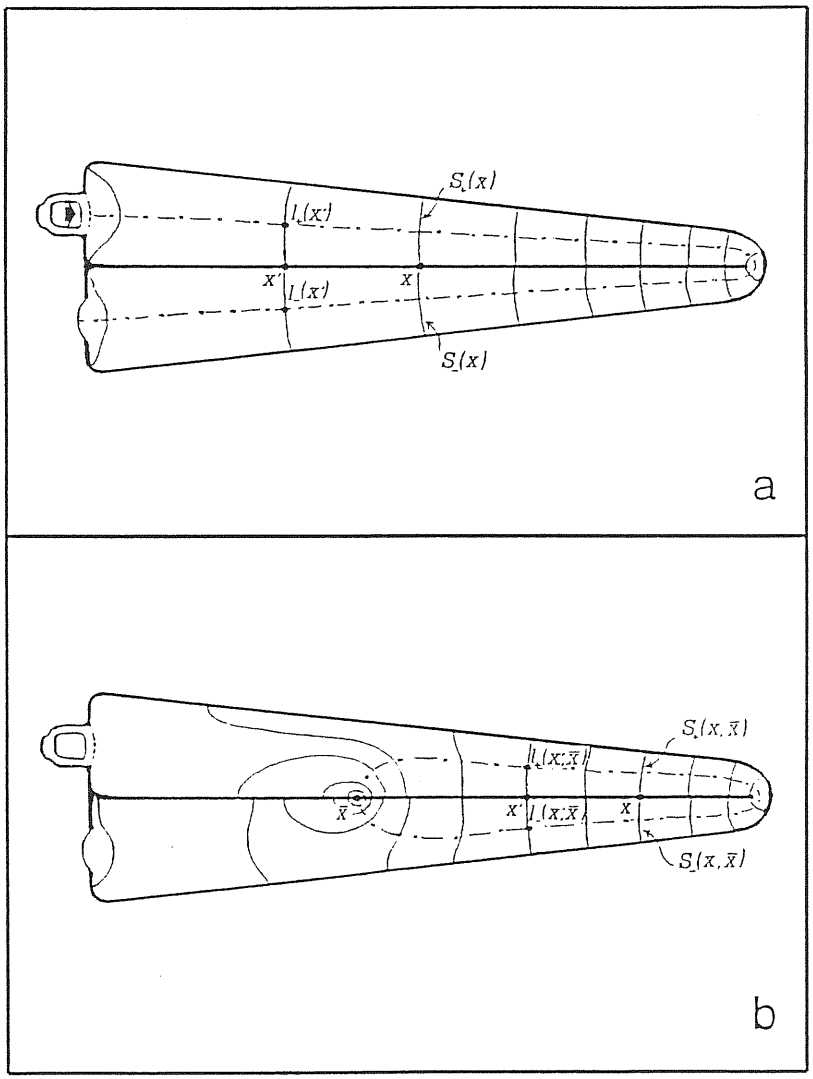

Figure 2.1: Isopotential surfaces of the fluid velocity field,
and related medial lines, generated (a) by the motion of the stapes, (b) by the motion of a BM segment at $\bar{x}$.

Let us indicate respectively by $p_+(x,t)$ and $p_-(x,t)$ the fluid pressure immediately above and below the BM segment at point x and time t, and with $\phi_+(x,t)$ and $\phi_-(x,t)$ the corresponding kinetic potentials. Then, Eq. (2.5) gives the following expression for the total force caused by the motion of the cochlear boundary

$$\begin{aligned} F_S(x,t) + F_{BM}(x,t) &= b(x)\,[p_-(x,t) - p_+(x,t)] \\ &= \rho\, b(x) \frac{\partial}{\partial t}\,[\phi_+(x,t) - \phi_-(x,t)]\ , \end{aligned} \tag{2.6}$$

where $b(x)$ is the BM width as defined below formula (2.1). So, provided the kinetic potentials just above and below x are known at any time t, the hydrodynamic effects of the cochlear motion are completely determined. This can be formally obtained as follows.

As long as the vibrating fluid boundaries do not change their average position, all the isopotential surfaces of ϕ do not depend on t. Let us indicate by $S_+(x)$ and $S_-(x)$ such surfaces intersecting the BM at x, respectively from above and below, as well as their areas. Since vector field $\vec{v}(\vec{r},t)$ is solenoidal, its instantaneous space–averaged values $\bar{v}_+(x,t)$ and $\bar{v}_-(x,t)$, respectively orthogonal to $S_+(x)$ and $S_-(x)$, satisfy the constant–flux condition $\bar{v}_\pm(x,t)S_\pm(x,t) = \text{const}$. Let $l_+(x)$ be the curvilinear coordinate along the medial line crossing the family of surfaces $S_+(x)$ from base ($x = 0$) to apex ($x = 1$) and $l_-(x)$ the coordinate across family $S_-(x)$ from apex to base (Fig.2.1a). Then

$$\phi_\pm(x_2,t) - \phi_\pm(x_1,t) = \int_{x_1}^{x_2} \bar{v}_\pm(x,t)\, dl_\pm(x)$$

$$= S_\pm(x_1)\bar{v}_\pm(x_1,t) \int_{x_1}^{x_2} \frac{dl_\pm(x)}{S_\pm(x)}\,.$$

To determine $F_S(x,t)$ we integrate $\phi_+(x,t) - \phi_-(x,t)$ in Eq. (2.6) along $l_+(x)$ from $x = 0$ to x, which yields the stapedial term of the kinetic potential

$$\phi_{S+}(x,t) = S\,\dot{\sigma}(t) \int_0^x \frac{dl_+(\bar{x})}{S_+(\bar{x})} + C$$

$$\phi_{S-}(x,t) = S\,\dot{\sigma}(t) \left[\int_0^1 \frac{dl_+(\bar{x})}{S_+(\bar{x})} + \int_1^x \frac{dl_-(\bar{x})}{S_-(\bar{x})} \right] + C$$

where S and $\sigma(t)$ are the surface and the displacement of the stapes, respectively,

and C is an integration constant. Defining

$$G_S(x) \equiv \rho\, b(x) S \int_x^1 \left[\frac{dl_+(\bar{x})}{S_+(\bar{x})} + \frac{dl_-(\bar{x})}{S_-(\bar{x})} \right] , \tag{2.7}$$

we obtain an explicit expression for Eq. (2.2).

In a similar way we can formally determine the contribution $\phi_+(x,\bar{x},t) - \phi_-(x,\bar{x},t)$ to the kinetic potential due to the acceleration $\ddot{\xi}(\bar{x},t)$ of a BM segment centered at $\bar{x}$ with length $d\bar{x}$. Let $S_\pm(x,\bar{x})$ be the families of equipotential surfaces of the kinetic potential generated by the motion of this segment and $l_\pm(x,\bar{x})$ their medial curvilinear coordinates (Fig.2.1b). These surface families differ significantly amongst themselves, depending on coordinate $\bar{x}$. Then, the $\bar{x}$–segment contribution to $F_{BM}(x,t)$ is proportional to $d\bar{x}$ multiplied by

$$G(x,\bar{x}) \equiv \rho\, b(x)\, b(\bar{x}) \int_x^1 \left[\frac{dl_+(x,\bar{x})}{S_+(x,\bar{x})} + \frac{dl_-(x,\bar{x})}{S_-(x,\bar{x})} \right] . \tag{2.8}$$

This provides an explicit expression for Eq. (2.3).

Of course, finding out, using the procedure just described, what the exact isopotential surfaces for a given cochlear boundary shape are, is rather a difficult task. This procedure, in fact, can only help us to understand the behaviour of the hydrodynamic propagators from a qualitative standpoint. Exact expressions could be derived for fluid boundaries with simple symmetry properties. For instance, Allen (1977) solved this problem for a cochlear duct with a constant rectangular cross–section. For a different geometry, Allen's result is valid only in the limit $x \to \bar{x}$, where the effect of the cochlear–duct boundary are strongly depressed. In this limit, $G(x,\bar{x})$ develops a logarithmic singularity of the type $\ln(r(x)/|x-\bar{x}|)$, where $r(x)$ is of the order of magnitude of the cochlear–duct radius at x.

We determined quantitatively approximate expressions of $G(x,\bar{x})$ following a different route, i.e. by an empirical procedure. The idea was that of working with an electrical analog of the fluid pressure field. We used a uniformly–tapering tube divided in two halves separated by a layer of insulating material. The two compartments were filled with saline solution and communicated at the most narrow tube end. On each face of the insulating sheet, copper strips were layed down transversally, forming 70 electrode couples. Function $G(x,\bar{x})$ was then obtained by passing

a fixed amount of alternating current through a given electrode couple whilst measuring the potential difference across all other couples, electrical potential replacing kinetic potential ϕ. Since this type of measurement depends on the geometry of the system, the model was designed as a faithful scaled representation of the uncoiled cochlear duct. The behaviours of $G_S(x)$ and $G(x,\bar{x})$ inferred from experiments on the electrical analog, as well as from theoretical consideration, are reproduced in Fig.2.2.

The analytical expressions we used in computations are

$$G(x,\bar{x}) = b(x)\,b(\bar{x})\,[G_o(x,\bar{x}) + P_o(x,\bar{x})]\ ,$$

and

$$G_S(x) \propto G(0,x)$$

where $b(x)$ is the BM width defined previously,

$$G_o(x,\bar{x}) = \begin{cases} p - q\,\bar{x} & \text{for } 0 \le x < \bar{x} \\ p - q\,x & \text{for } \bar{x} \le x \le 1 \end{cases}\ , \qquad (2.9)$$

with $p \approx 30$ and $q \approx 28$, and

$$P_o(x,\bar{x}) = \begin{cases} c\,\ln(r(x)/|x-\bar{x}|) & \text{for } |x-\bar{x}| < r(x) \\ 0 & \text{otherwise} \end{cases}\ , \qquad (2.10)$$

with $c \approx 0.125$. It is not necessary to justify the choice of these values for the constants p, q and c since the normalisation of $G(x,\bar{x})$ is merely conventional. The effective cochlear radius $r(x)$ represents the cutoff of the logarithmic singularity due to the proximity of the cochlear–duct boundary. We estimated it as

$$r(x) \approx 0.04 - 0.02\,x$$

by comparing the area under each peak to the measured amplitude of the corresponding discontinuity in the electrical potential. As far as the relative magnitude of $G(x,\bar{x})$ is concerned, we considered that

$$\overline{G} = \int_0^1 \int_0^1 G(x,\bar{x})dx\,d\bar{x}$$

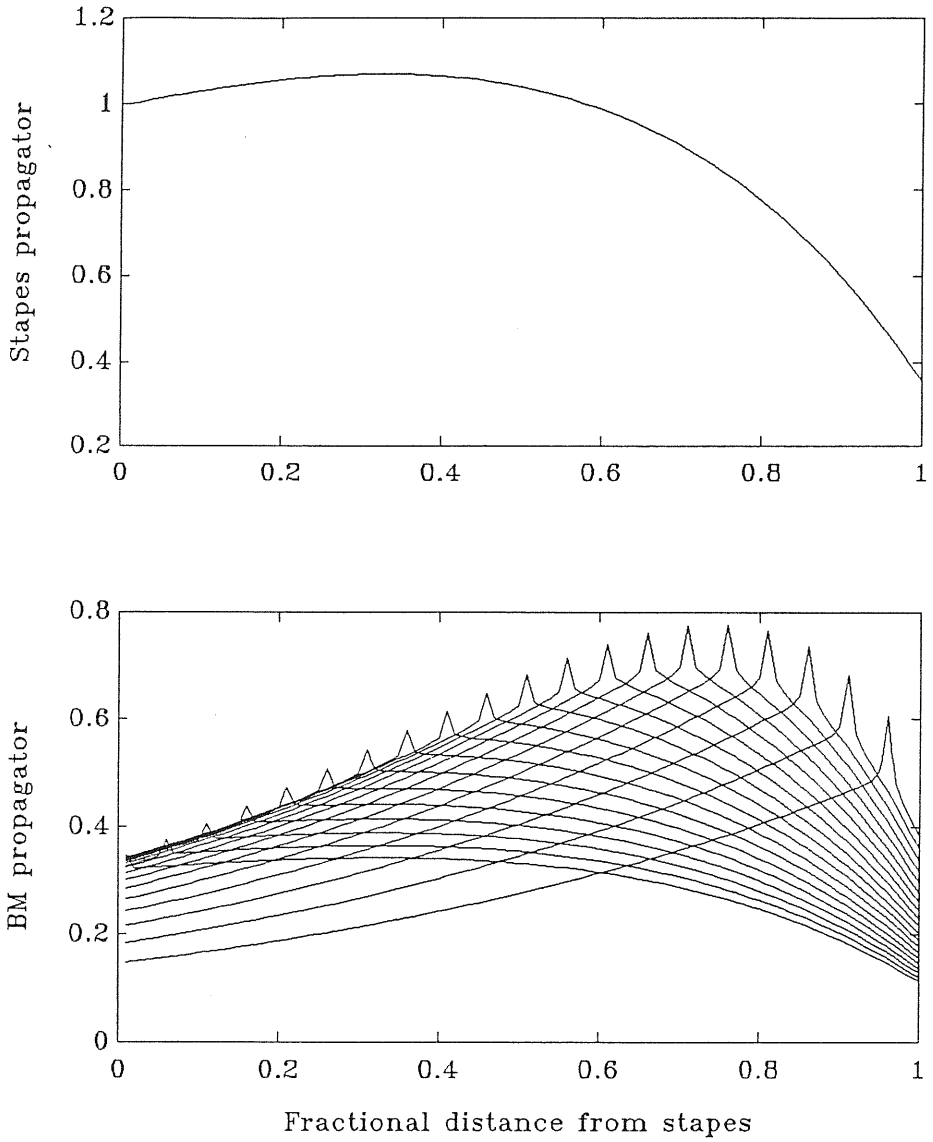

Figure 2.2: Hydrodynamic inertial propagators

as functions of the BM position–variable x. (a) $G_S(x)$: hydrodynamic propagator of the stapes motion (Eq.2.7). (b) $G(x, \bar{x})$: hydrodynamic propagator of the motion of the BM–segment at $\bar{x}$, for $\bar{x} = n/20$, $n = 1, 2, \ldots 20$, (Eq.2.8).

is the hydrodynamical mass loading the BM when the membrane is rigidly displaced all along its length. Hence we assumed

$$\overline{G}/\overline{M} \approx 20\,, \qquad \text{with} \quad \overline{M} = \int_0^1 m(x)\,dx\,. \tag{2.11}$$

$\overline{M}$ is the the total mass of the organ of Corti. This figure corresponds roughly to the ratio of the cochlear diameter divided by thickness of the organ of Corti. The inertial character of both the hydrodynamic propagators is evident in that $G_S(x)$ and $G(x,\bar{x})$ have the dimension of mass per unit length and per unit surface respectively. We assume that $G_S(x)$ is well approximated by $G(x,0)$, except for a proportionality constant, as this is tantamount to assuming that the kinetic field generated by the stapes is similar to that generated by the most basal BM segment.

2.4 Travelling waves in the passive cochlea

Separating the non–homogeneous term representing the external signal from the homogeneous terms depending on ξ and ignoring the space–derivative terms for reasons previously discussed, the law governing the BM motion in the absence of active processes is

$$\begin{aligned}&\int_0^1 G(x,\bar{x})\,\ddot{\xi}(\bar{x},t)\,d\bar{x} + m(x)\,\ddot{\xi}(x,t) + h(x)\,\dot{\xi}(x,t) + k(x)\xi(x,t)\\ &= -G_S(x)\ddot{\sigma}(t)\,.\end{aligned} \tag{2.12}$$

Denoting by $\tilde{a}(\omega)$ (or, when more convenient, by $\tilde{a}_\omega$) the Fourier–transform of a generic time function $a(t)$, Eq. (2.12) can be equivalently stated as

$$\begin{aligned}&-\omega^2\left[\int_0^1 G(x,\bar{x})\,\tilde{\xi}(\omega,\bar{x})\,d\bar{x} + m(x)\,\tilde{\xi}(\omega,x)\right] + i\omega\,h(x)\,\tilde{\xi}(\omega,x) +\\ &k(x)\tilde{\xi}(\omega,x) \;=\; \omega^2\,G_S(x)\,\tilde{\sigma}(\omega)\,.\end{aligned} \tag{2.13}$$

We can express this equation in a more compact form defining the kernel

$$K_\omega(x,\bar{x}) \;=\; \delta(x-\bar{x})\left[k(x) + i\omega h(x) - \omega^2 m(x)\right] - \omega^2 G(x,\bar{x})\,,$$

where $\delta(x-\bar{x})$ is Dirac's delta. The simplified Fourier–transformed Eq. (2.13) is then

$$\int_0^1 K_\omega(x,\bar{x})\,\tilde{\xi}(\omega,\bar{x})d\bar{x} \;=\; \omega^2 G_S(x)\,\tilde{\sigma}(\omega)\,. \tag{2.14}$$

This integral equation can be solved for $\tilde{\xi}(x,\omega)$ by standard numerical methods, provided functions $m(x)$, $k(x)$, $h(x)$, $G(x,\bar{x})$, $G_S(x)$ are known. These have been determined in section 2.3 except for their proportionality constants and for the exponent α of $h(x)$. Three of these constants can be freely chosen: one because the equation is linear; another because the amplitude of $\tilde{\sigma}(\omega)$ is arbitrary; the third one because the dimension of ω can be rescaled. The constant for $m(x)$ has been chosen to be equal to 0.125 in order for Eq. (2.11) to be fulfilled. We chose the others in such ways that $G_S(0) = 1$ and $k(0.5) = 1$. Finally, α and the proportionality constant of $h(x)$ were empirically determined by the condition that the solutions of Eq.2.14 match the passive waveforms observed by von Békésy in cochleas from cadavers. We assigned $\alpha \approx 0.92$.

A typical solution of Eq. (2.14), representing the BM response to a pure tone is shown in Fig.2.3a and should be compared with the TWs found by von Békésy (see Fig.1.3a). In Figs.2.3b,c various TW amplitude envelopes and phases are plotted for a set of frequencies ordered in a decreasing geometric progression (from left to right) and for a constant velocity at the stapes. Note that frequency changes make the curve translate along the BM with amplitudes scaling approximately as the square of the frequency. The values of coordinate x at which the TW maxima occur are mapped onto corresponding stimulation frequencies, i.e. the *characteristic frequencies* of x, as expected, according to a logarithmic law.

2.5 The role of outer hair cells

The main physiological facts concerning the behaviour of OHCs are here briefly summarized:

OHCs contract when their membranes are depolarized and elongate when they hyperpolarized. In response to voltage steps, these cells change length with a very fast exponential time course, having a characteristic time–constant as small as 240 μsec. Maximal length changes are of the order of 4–5 % of the cell length. Basal cells are about 20 μm long and apical cells about 80 μm. The peak sensitivity of the motile response is approximately 20 nm/mV (Ashmore, 1987).

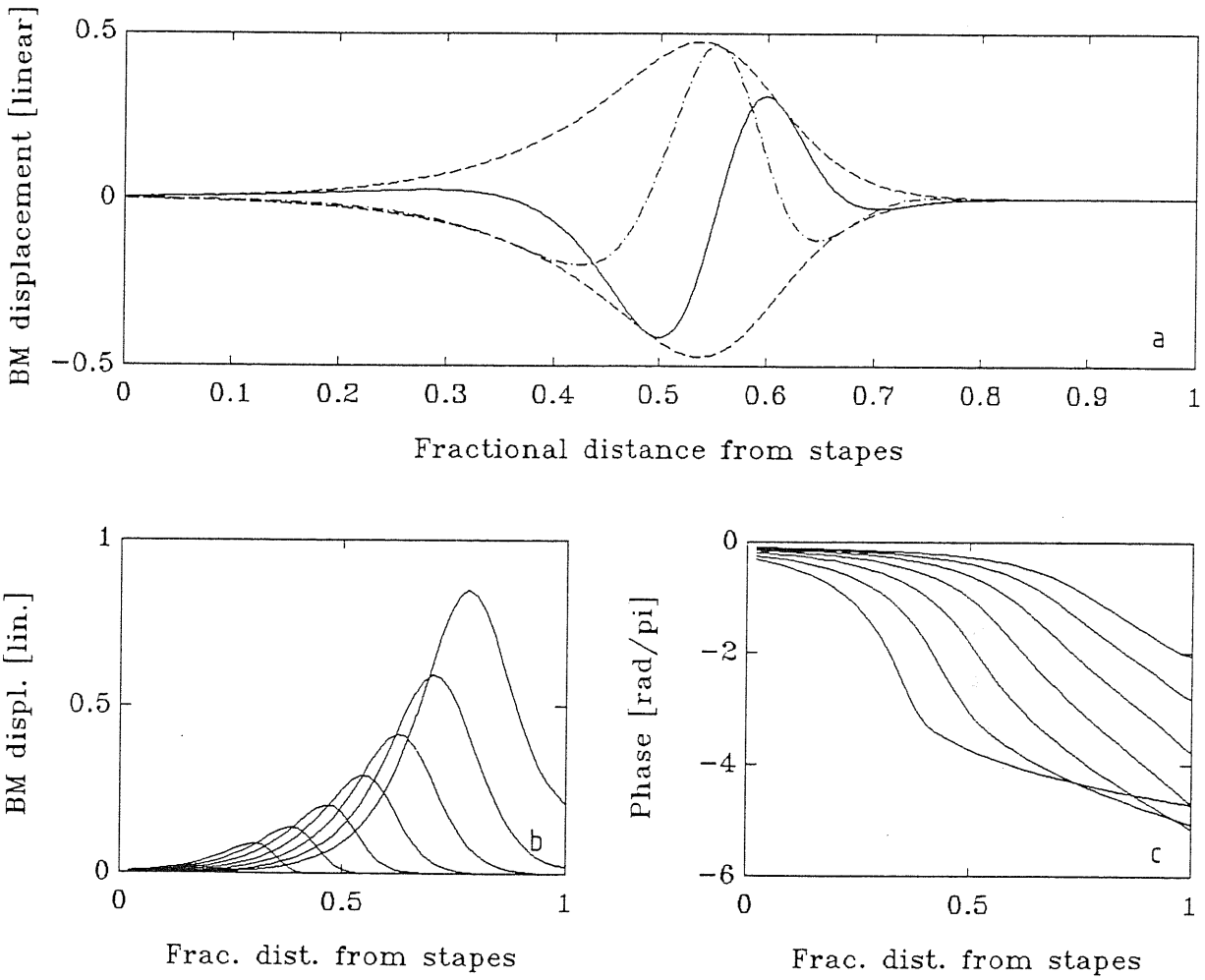

Figure 2.3: Solutions of the motion equation for the passive cochlea obtained from Eq.2.14. (a) Solid line: real part; dash–dot line: imaginary part; dashed line: amplitude envelope. (b) Amplitude profiles elicited for sound frequencies decreasing in geometrical progression from left to right and a constant velocity at stapes. (c) Corresponding phases (in units of π).

The frequency response of the OHC membrane–potential, which controls the OHC mechanical transduction, measured both *in vivo* (Dallos, 1985) and *in vitro* (Housley and Ashmore, 1989), approximately displays a low–pass–filter characteristic with a cutoff frequency $\omega = (RC)^{-1}$ determined by capacitance C and resistance R of the cell–membrane. From experiments on isolated cells *in vitro* the slope conductance of the basolateral OHC membrane at resting potential is known to decrease from 51 nS in cells from the base to 3.6 nS in those from the apex, while the cell capacitance increases linearly from about 18 pF at the base to about 45 pF at the apex. Quantitatively, the OHC cutoff frequencies appear to vary by less than one order of magnitude from base to apex, the highest cutoff not exceeding about 700 hertz.

Measurements of the longitudinal mechanical stiffness of isolated OHCs (Holley and Ashmore, 1988) show that OHCs are robust enough for their motility to have appreciable mechanical effects within the organ of Corti. Thus, as long as the cell motility is ignored, OHCs provide a small additive contribution to the passive mechanical stiffness of the organ of Corti. When OHC motility, triggered by the BM motion, is taken into account, an effective–contribution to the BM stiffness, possibly time–delayed, is to be expected. In fact, in the linear approximation, the OHC triggering establishes a proportionality relationship between the local displacement of the organ of Corti and some form of actively generated force applied to the BM. In principle, the sign of this contribution may be positive or negative depending on the micromechanics of the organ of Corti. According to the geometry of its supporting cells, the organ of Corti should comprehensively *lower* when the RL and the BM (between which the OHCs are inserted) are forced to approach each other by cell contraction (Fig.2.4). We assumed that this is the case and that membrane–potential changes are caused by deflection of the stereocilia (as it is largely believed). Then we concluded that upwards (downwards) movements of the BM, forced by external pressure, cause stereocilia deflection (relaxation), hence cell-contraction (elongation), thus eliciting an additive pseudo–elastic reaction. We assessed this with a simple mechanical model of a segment of the cochlear partition, from which we also learned that, under OHC contractions or elongations, the tract of BM fibres spanning from the insertion point of OHCs to the outer cochlear wall remains approximately in the same position, whereas the largest displacement of

the organ of Corti occurs at the OPCs footplate.

At least from a static point of view, the forces applied by OHCs, as noted above, are of the right magnitude to provide the requisite dynamic control of the BM mechanics. Then, in principle, the response rapidity would enable these forces to act over the cochlear partition on a cycle–by–cycle way at all audible frequencies. The pivoting of the OHC stereocilia, as caused by TW propagations, would thus result in a feedback action of the cells over the BM, so as to compensate for the energy loss due to viscosity. As a consequence, the TW should be boosted and become sharply tuned (Ashmore, 1990).

Because of the cutoff mentioned above, the OHC responses to deflection of the stereocilia are strongly depressed at high frequencies. This would prevent the OHCs from effectively undamping the cochlear dynamics at frequencies above 700 Hz. How could this shortcoming ever be circumvented in the cochlea *in vivo*? In our opinion this question is answered simply: since, at high frequencies, a low–pass–filtered signal–amplitude varies as the inverse of frequency, whereas the viscous force is proportional to frequency, *the OHC triggering mechanism must depend on a factor proportional to the square of frequency, what amounts to assuming the presence of an inertial effect.*

The above considerations enable us to envisage a well–defined expression for the undamping term to be added to the l.h.s. of Eq. (2.14). This term is even univocally determined provided it is also considered that the BM responses observed in vivo under whatever sound stimuli always occur at the threshold of spontaneous oscillations (Kemp, 1978; Wilson, 1980). This implies that the energy dissipation factors affecting the passive cochlear motions are always *exactly neutralized but not overcompensated* by the underlying active processes.

Hence we arrive to establish the undamping force term as

$$U_\omega(x) = \frac{a_\omega(x)}{\omega_c(x) + i\omega}\,\tilde{\xi}(\omega, x)\,,$$

where $a_\omega(x)$ is the aforementioned OHC triggering–factor (to be determined) and $\omega_c(x)$ the cutoff–frequency of the OHCs at x. On the basis of the known properties

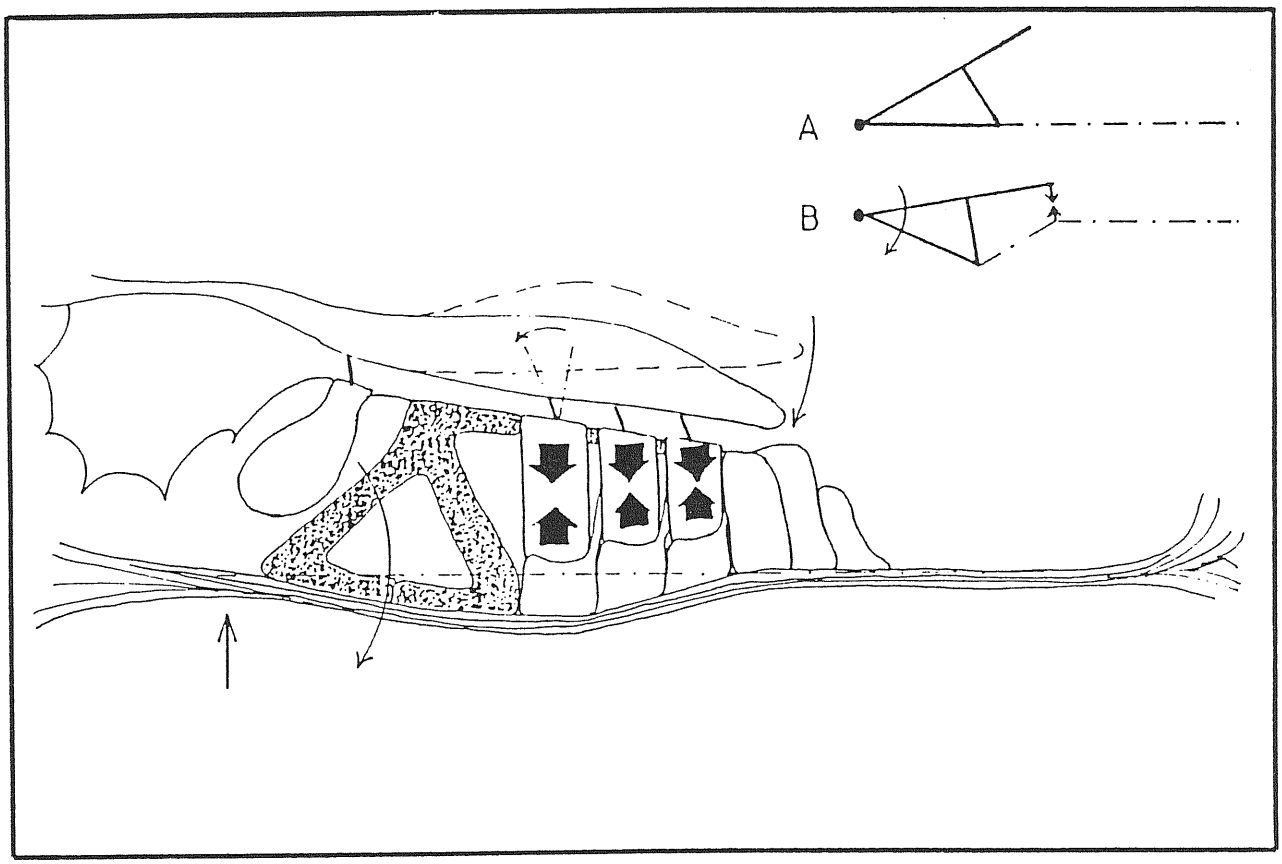

Figure 2.4: Putative action of the OHCs on the cochlear partition.
When OHCs contract (relax), the RL and the BM are forced to approach (depart from) each other. Consequently, the whole organ of Corti lowers (rises), pivoting around the base foot of IPC (a → b). The tectorial membrane (TM) is separated from the reticular lamina (RL) by a narrow fluid–filled space and is linked to the latter by the tips of the highest OHC stereocilia. The organ–of–Corti's lowering (rising) causes the TM to shear with respect to the RL, the stereocilia to straighten (deflect towards the external border of TM) and, consequently, the OHCs to relax (contract). Since the effect is always such as to contrast the cause, the system admits a state of equilibrium at an intermediate degree of OHC contraction.

of OHCs, we expresses this as

$$\omega_c(x) = \omega_o \exp(-\gamma x); \qquad \omega_o = 0.812; \quad \gamma = 2.326,$$

where the value of ω_o corresponds to 700 hertz in our units. By examination of the TWs obtained as solutions of the equation for the passive cochlea we can assess that, for frequencies that are not too low, the TWs differ appreciably from zero only over a BM tract for which $\omega_c(x) \ll \omega$. Then, in these conditions, $U_\omega(x)$ can be approximated as

$$U_\omega(x) \approx -i \frac{a_\omega(x)}{\omega} \tilde{\xi}(\omega, x), \tag{2.15}$$

which forces us to assume $a_\omega(x) \propto \omega^2$ if the damping term $i\omega\, h(x)\, \tilde{\xi}(\omega, x)$ in Eq.2.13 (due to the TM cleft resistance) is to be cancelled for frequencies that are not too low. At low frequency the cancellation will be only partial, consistently with the experimental finding that the tuning properties of the cochlea are worse in the apical region.

2.6 The role of the stereocilia stiffness

In section 1.2 the comprehensive pivotal stiffness of all the stereocilia which belong to the same cochlear segment was estimated to be larger than 0.1 N/m. Considering that the bundles of stereocilia, especially at the base of the cochlea, are stressed by forces applied in directions forming small angles with the OHC longitudinal axis, the *effective* bundle stiffness, relative to the vertical BM displacement, is expected to greatly exceed 1 N/m at the base and gently decrease from this value towards the apex of the cochlea. Since this figure is at least one order of magnitude larger than the maximum fibre stiffness of a BM segment, everything works as if the TM were rigidly connected to the organ of Corti. As far as the mechanical properties of the cochlea are concerned, this would simply provide an additional mass to the cochlear segments, but this large stiffness value has important implications for the frequency dependence of the OHC triggering mechanism. We can realize this on a simple model which accounts for the elastic reaction of a TM tract to the motion of a BM segment.

Let us consider an harmonic oscillator (not subject to gravitational forces, for the sake of simplicity) formed by a spring with stiffness k and damping constant h, attached to a mass m at one end. Let $x(t)$ and $y(t)$ be the extreme coordinates of the spring, where $x(t)$ is a prescribed function of t, while $y(t)$, adjacent to the mass, follows the system dynamics. Defining the spring elongation as $z(t) = y(t) - x(t)$, the motion equation is

$$m\,\ddot{z}(t) + h\,\dot{z}(t) + k\,z(t) = -m\,x(t)\,.$$

The Fourier transform of $z(t)$ is

$$\tilde{z}_\omega \;=\; \frac{\omega^2\, m\, \tilde{x}_\omega}{k + i\,\omega\, h - \omega^2\, m}\,,$$

where Fourier–transformed quantities are defined as usual. Now we interpret $x(t)$ as the displacement $\xi(x,t)$ of the BM segment at x, $z(t)$ *as the height of the subtectorial gap*, k as the effective stiffness constant of the stereocilia bundles of a BM segment, h as the TM cleft resistance and m as the mass of the TM segment facing the BM segment. Then, provided $k \gg \omega^2\, m$ and $k \gg \omega\, h$, the spring elongation $\tilde{z}_\omega$ is actually proportional to ω^2. Taking $\approx 10\mu$m as the length of a BM segment, $\approx 10^{-6}$ kg/m as the TM mass per unit length and 0.0015 Nsec/m^2 as the perilymph viscosity (these figures refer to the guinea–pig cochlea), the above inequalities are satisfied for frequency values up to ≈ 40 kHz (which covers most the range of audible frequency for the guinea–pig). As it is reasonable to assume that the OHC triggering is proportional to $z(t)$, i.e. to the deflection of the stereocilia, the required dependence of $a_\omega(x)$ on ω^2 in Eq. (2.15) is justified. Hence, in order for the fluid viscosity term $i\,\omega\, h(x)\,\tilde{\xi}_\omega(x)$ in Eq.2.13 to be uniformly cancelled over the whole cochlear length and for all frequencies that are not too low, the following relationship must hold

$$a_\omega(x) \approx \omega^2\, h(x) \;\propto\; \omega^2\, \exp(-0.92x).$$

Note that $a_\omega(x)/\omega^2$ decreases only about 2.5 times from base to apex, which is consistent with a moderate change in the static sensitivity of the OHC triggering. Therefore we establish the undamping term as

$$U_\omega(x) \;=\; \frac{\omega^2\, h(x)}{\omega_c(x) + i\omega}\,\tilde{\xi}(\omega, x)\,.$$

2.7 Travelling waves in the active cochlea

On the basis of the previous section, the kernel for the active–cochlea equation can be put in the form

$$H_\omega(x,\bar{x};\,\lambda) \;=\; K_\omega(x,\bar{x}) + \lambda\,\delta(x-\bar{x})\,\frac{\omega^2\,h(x)}{\omega_c(x)+i\omega}\,,$$

where $\lambda \in [0,1]$ is a parameter introduced in order to control the amount of residual damping and represents the degree of efficiency of the OHCs. As λ approaches 1, the undamping become almost complete for any frequency that is not too low, without violating the stability conditions of the system, what assures the *structural stability* of the cochlear function.

The plots in Fig.2.5 show numerical solutions $\tilde{\xi}(\omega,x)$ of the equation

$$\int_0^1 H_\omega(x,\bar{x};\,\lambda)\,\tilde{\xi}(\omega,\bar{x})d\bar{x} \;=\; \omega^2 G_S(x)\,\tilde{\sigma}(\omega)\,, \tag{2.16}$$

obtained for various values of λ. Both the enhancement and the remarkable shrinking of the TW head, as well as its forward displacement, are evident. A noteworthy feature is the small difference between the phases of the TWs in the passive and active cases. This result agrees with the fixed–site variable–frequency experimental data of Robles *et al.* (1986) and Ruggero and Rich (1991). They showed that, as the conditions of the cochlea worsen, the amplitude of the response decreases whereas the phase lags back by at most one cycle, at the characteristic frequency of the site. Translating this into variable–site fixed–frequency conditions, the phase should remain almost constant up to the point where the TW peaks. It is worth mentioning that other authors have been able to obtain TWs with correct amplitude profile, but their phases depart from experimental data (see e.g. Neely and Kim, 1986). The breakdown of the phase profile and the lack of structural stability seem to be common features of all the models including negative–damping terms or secondary resonators within the organ of Corti. In our model, realistic phases are obtained only with the condition that the undamping term *never* introduces negative–damping corrections to the passive dynamics.

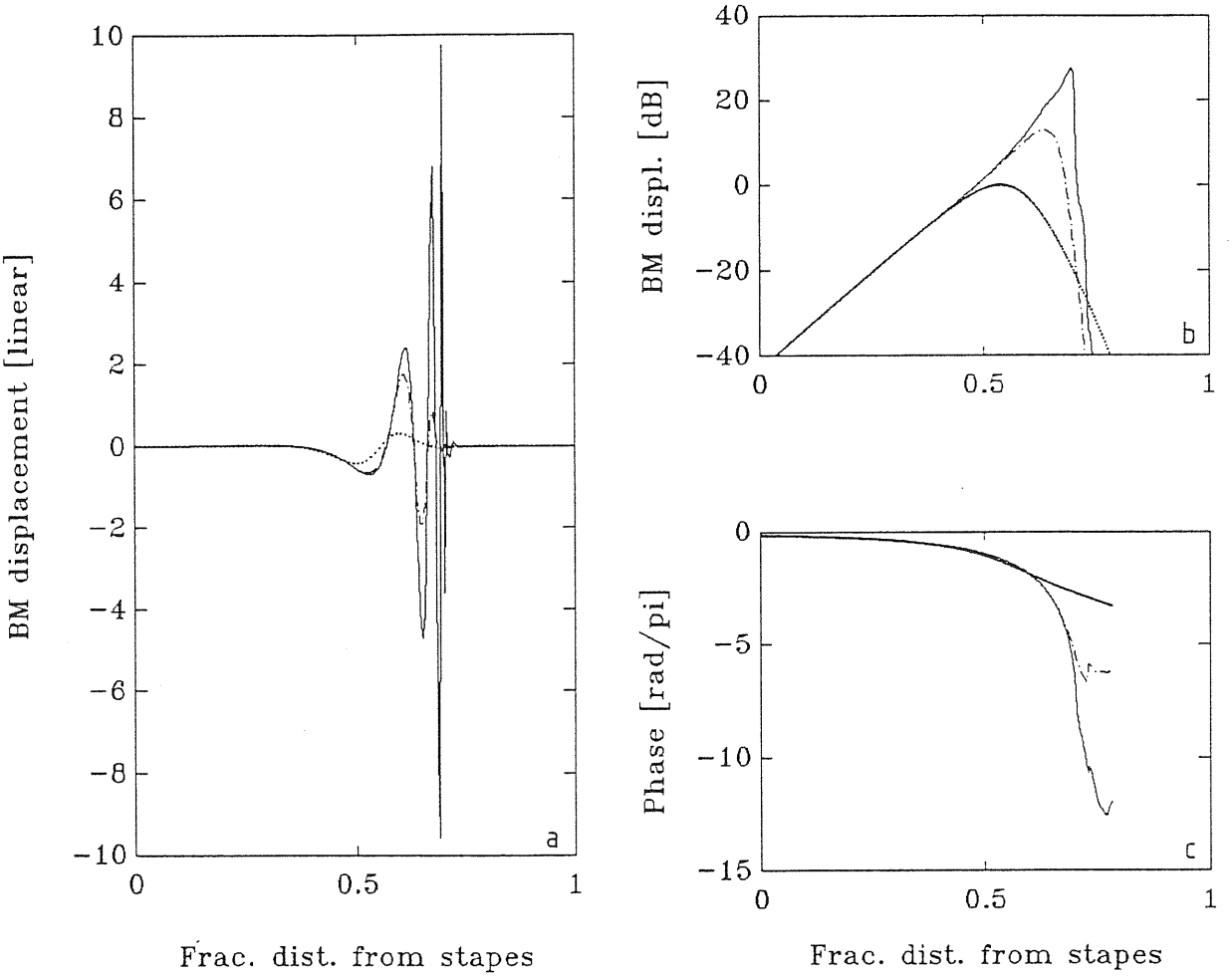

Figure 2.5: Solutions of the TW equation for the active cochlea obtained from Eq.2.16 for various values of the damping–control parameter λ, with all other parameters as in Fig.2.3. Dotted lines: $\lambda = 0$, giving the same TW shown in Fig.2.3a (on a different scale); dash–dot lines: $\lambda = 0.9$; solid line: $\lambda = 0.99$. (a) Real parts of the solutions plotted on a linear scale. (b) The corresponding amplitude profiles are shown on a decibel scale. (c) Phases in units of π.

2.8 Summary

We present here a new approach to cochlear dynamics. The work has been developed in strict adherence to the physiological data and through an accurate analysis of the cochlear fluid dynamics. The prevalence of the hydrodynamic coupling and of the BM fibre stiffness over the longitudinal viscoelastic coupling represented by space–derivate terms has made it possible to reduce the law governing both passive and active cochlear dynamics to an integral equation. The extraordinary frequency selectivity of the active cochlea has been attributed to the role of undamping played by the motility of outer hair cells. As is well–known, the main problem concerning the effectiveness of these cells is that they behave as mechanical transducers with low–pass filter characteristics, together with the small values of their cutoff frequencies. On the other hand, cutoff frequencies higher than those experimentally found would be incompatible with the constraints imposed by the physics of biological systems. We have envisaged the expedient by which nature has been able to circumvent this difficulty in the inertial reaction of the tectorial membrane. In order for this mechanism to properly work, a large stereocilia bundle stiffness is required, which does seem to be the case.

The dynamical behaviour of the cochlea has been simulated through numerical solutions of the aforementioned integral equation. The computed amplitude–envelopes as well as the phase–profiles of the basilar–membrane responses to pure tones are in good agreement with the experimental data at low intensities, both for the passive and the active cases. Discrepancies arising at higher intensities can be interpreted as being due to the fact that our approach is limited to the linear approximation.

Chapter 3

Experiments

3.1 Abstract

In the previous chapter, the possibility that fluid damping of the cochlear partition is counteracted by motile responses of the outer hair cells (OHCs) was examined theoretically. However, direct experimental evidence that the forces generated by these cells are sufficient to affect the micromechanics of the cochlear partition has not yet been provided. This information is essential for the understanding of the filtering capabilities of the mammalian peripheral auditory system.

We investigated this hypothesis by stimulating the isolated cochlea by extracellular current whilst measuring, using a computer–controlled Michelson interferometer, the motion of silvered glass beads placed on the cochlear partition. The response of the basilar membrane (BM) to step–like stimuli was a damped oscillation. Larger amplitudes but qualitatively different dynamic responses were measured from beads placed on the tectorial membrane (TM), indicating that the tuning of the cochlear partition varies in the radial direction, for the same cochlear site. Frequency analysis was also performed on the BM by means of a lock–in–amplifier using sinusoidal stimuli in the range from 50 to 10000 Hz. Responses were labile.

3.2 Rationale for the experiments

If the OHC motility is to play any role in the mechanics of the cochlea, it must be possible to induce displacements of the cochlear partition by suitably stimulating the OHCs.

Motile responses can be elicited in isolated OHCs by intracellular current injection by the recording microelectrode (Brownell *et al.*, 1985) as well as by varying the holding potential of the patching pipette (Ashmore, 1987). However, a different approach is required for stimulating these cells *in situ*. The cochlear partition is almost completely transparent and the use of contrast–enhanced microscopy is prevented by having to illuminate the isolated cochlea with diffused light. Although "blind" insertion of microelectrodes in the organ of Corti permitted to record from both inner and outer hair cells (Dallos, 1985; Cody and Russel, 1987) it has not proved possible so far to patch–clamp a cell inside the cochlea. However, it is probably *a priori* inadvisable to insert an electrode inside the organ of Corti, for this certainly provides a mechanical bias to the extremely delicate micromechanics of the cochlear partition.

Brownell and Kachar (1985) showed that OHC motility can be elicited in isolated cells just by exposing them to the electric field generated by a pair of silver–wire electrodes placed in the bathing solution. OHC length changes can be detected optically at current levels of about 1mA. Dallos *et al.* (1991) "microchamber" technique is conceptually a refinement of Brownell's preparation. Assuming that the resting conductance of the cell's basolateral membrane is uniform, these experiments suggest that a net contraction or elongation of an OHC should be expected provided the *divergence* of the stimulating electric field is large enough to produce a non–homogeneous current flow across the cell membrane (Fig.3.1). This indicates that OHC–driven displacements of the cochlear partition should be observed in response to a diverging field of extracellular current intercepting the organ of Corti. Such a field can be easily created by using two electrodes of different size, and placing the thinner one in the proximity of the organ of Corti. The size of the stimulating electrode should be kept as small as possible, so that focal stimuli can be generated. If pipettes are used to pass extracellular current, the size of the expected displace-

ments of the cochlear partition should be in the range of 1–10 nm, as the largest current that can be passed with a pipette (without applying potentials larger than 10 V) is about 100 μA. Nanometre displacements are best detected by means of laser interferometry.

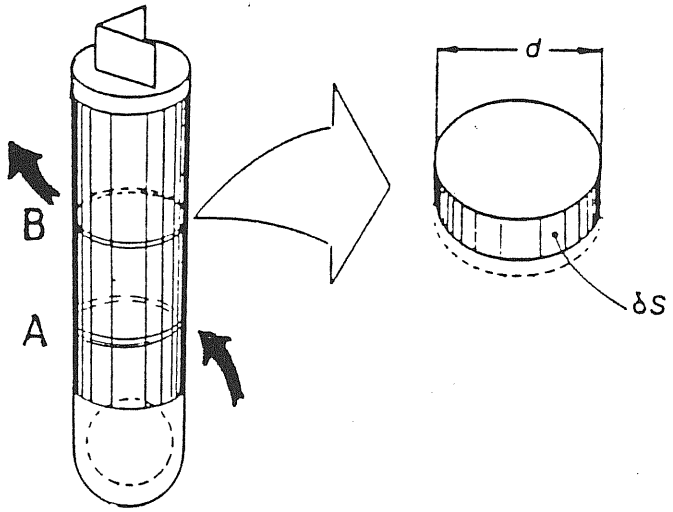

Figure 3.1: Effect of current on an outer hair cell

A cationic current of density I_a entering the cell at location A will decrement the potential drop acros the cell wall by $dV_a = R_m\, I_a d\sigma$, where $d\sigma$ is the area of an annular cell segment at A and R_m the cell–membrane resistance, assumed to be uniform. This will cause a longitudinal expansion of the cell segment proportional to dV_a. Current leaving the cell at B will produce a contraction of the corresponding annular segment proportional to $dV_b = R_m\, I_b\, d\sigma$. A net change in the comprehensive cell length will take place provided that the inflowing current density differs appreciably from the outflowing one, as a consequence of divergence in the driving electric field.

3.3 Methods

Dissection

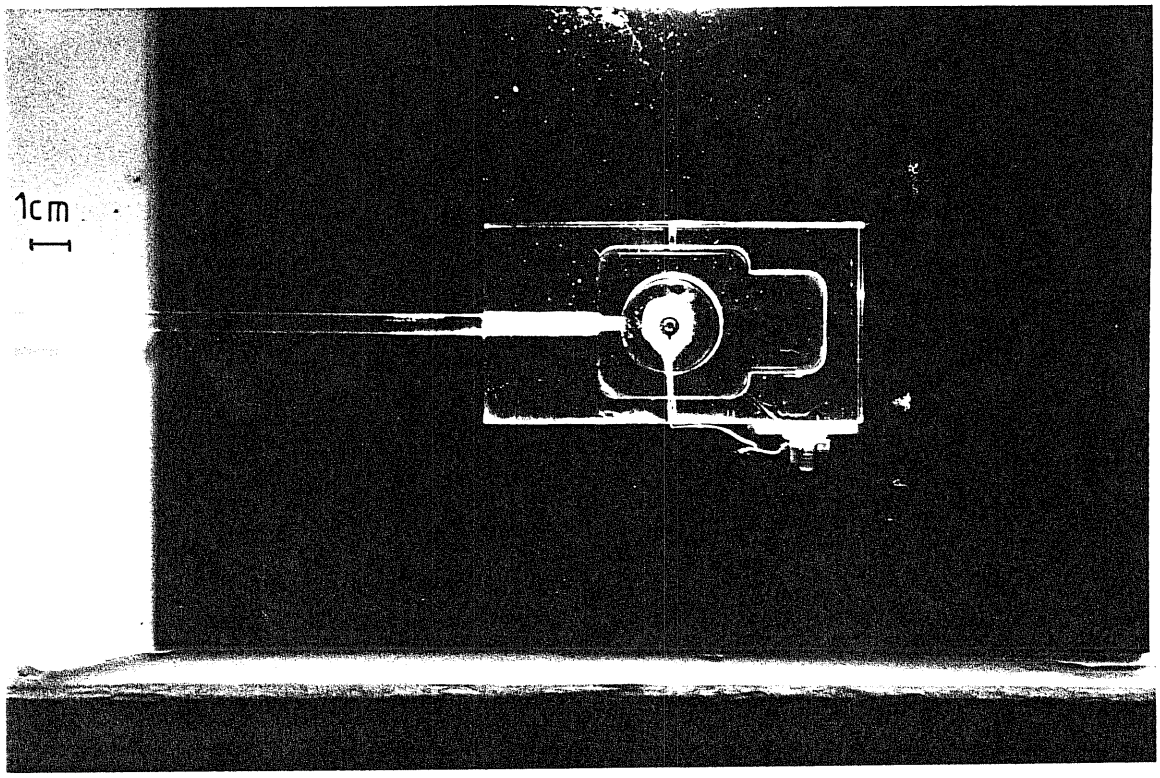

Figure 3.2: Photograph of the chamber

designed to hold the excised cochlea under a compound microscope. Scale bar: 1 cm.

Adult guinea–pigs (200–300 g) are killed by rapid cervical dislocation and both bullae removed. The cochlea is exposed by cracking one bulla and placed in a specially designed chamber filled with L–15 medium (lx, GIBCO; the major ions in the medium are (mM): Na^+, 145; K^+, 5; Ca^{2+}, 1.26; Mg^{2+}, 2; and amino acids; pH 7.4). The chamber (Fig.3.2) consists of a perspex slab in which a cylindrical well allows room for the cochlea. At the bottom of the well a large silver–cloride pellet is inserted as a reference electrode. Two capillary–size holes provide communication from the well to the perfusion system. The well is also endowed with a lateral hole, inside which a threaded rod can be rotated freely. The wall of the bulla is glued to a conventional nylon screw with rapid dental cement and held inside the chamber by fixing the screw to the rod.

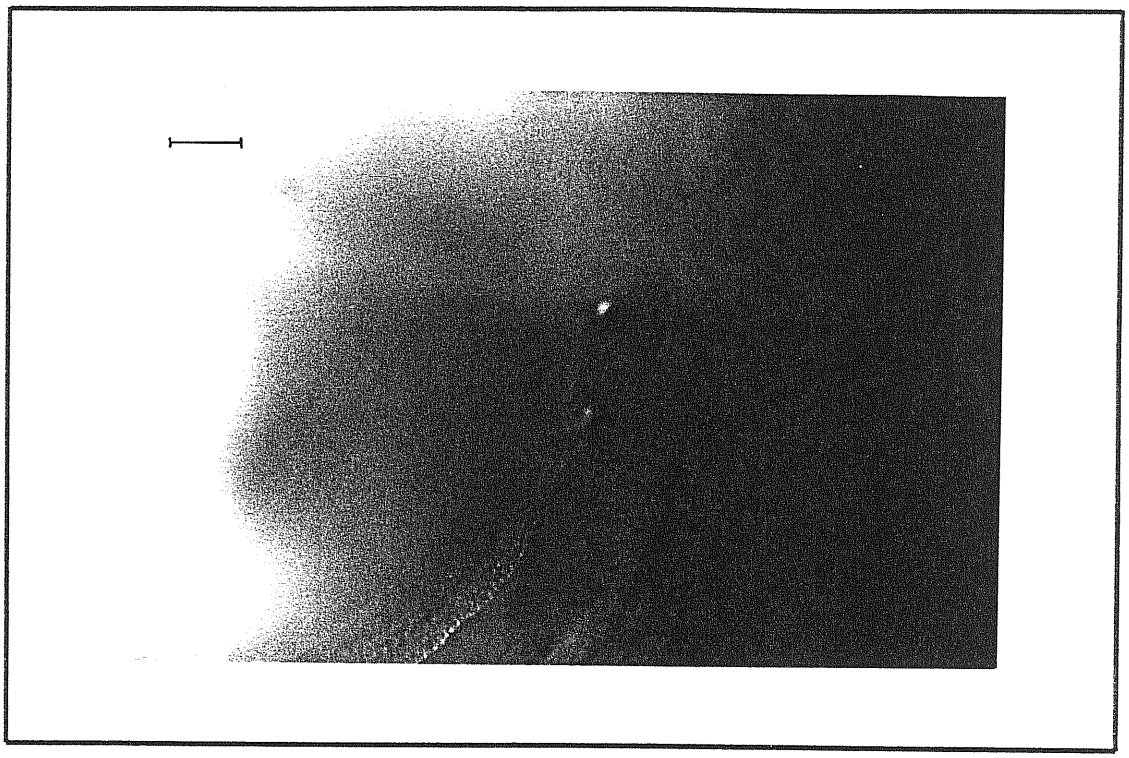

Figure 3.3: Photograph of the exposed apical turn of a guinea–pig's cochlea. Reflective beads are seen sitting over the cochlear partition. The lipid globules of the Hensens' cells mark the border between the organ of Corti and the BM. Scale bar: 100 μ.

The cochlear partition, viewed under a dissection microscope, is exposed from scala vestibuli by gently scraping the bony wall of the cochlea beginning with the apical turn. If it is desired to work in turns below the apical one, the modiolus is severed in the turn above that of interest. In this way it is possible to reach points of the BM as far as 10–11 mm from the helicotrema. The preparation is completed by carefully removing the Reissner's membrane with a hypodermic needle. Reflective beads are then dropped onto the cochlear partition (Fig.3.3). The beads are silvered glass spheres ranging in diameter from 10 to 50 μm.

Recording methods

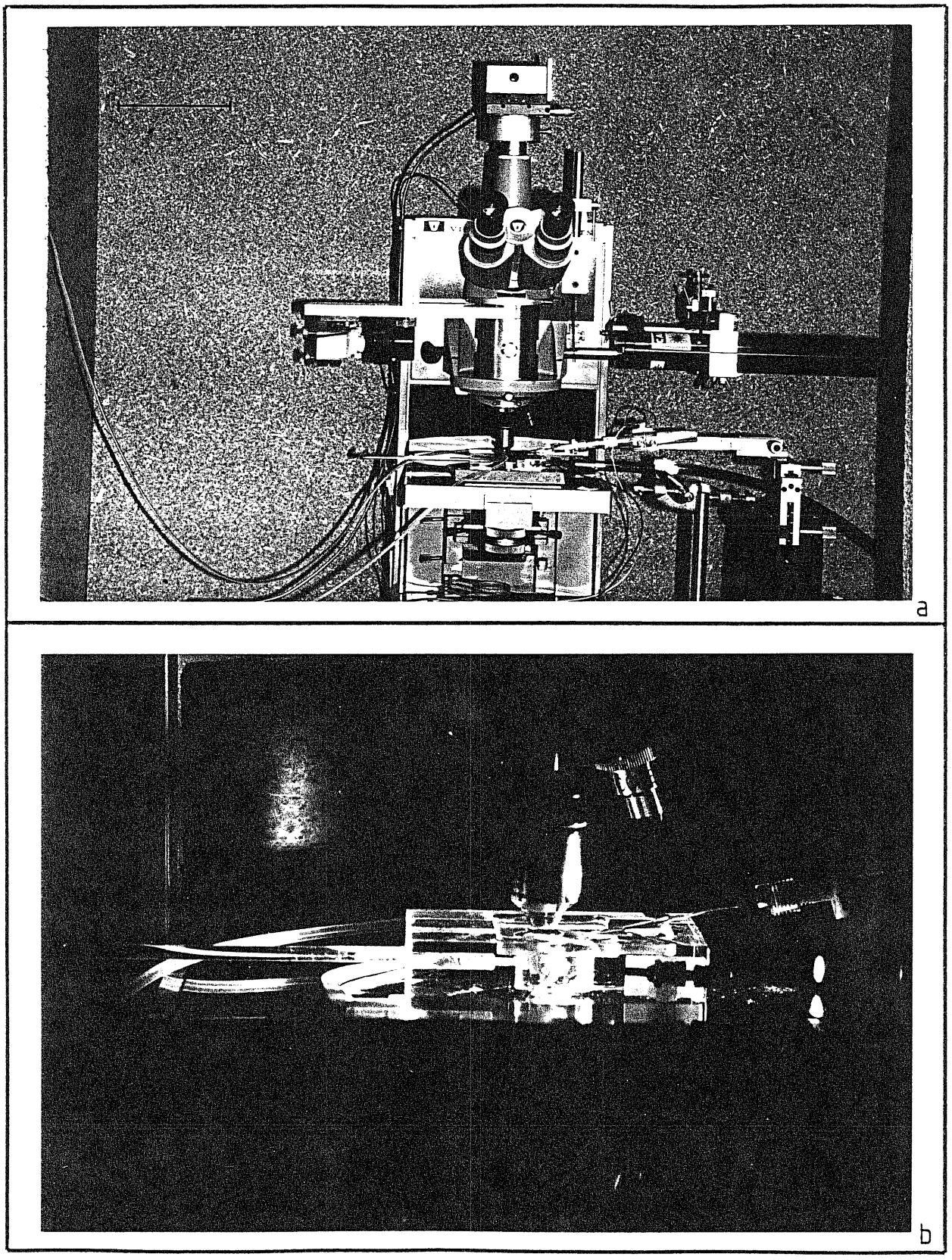

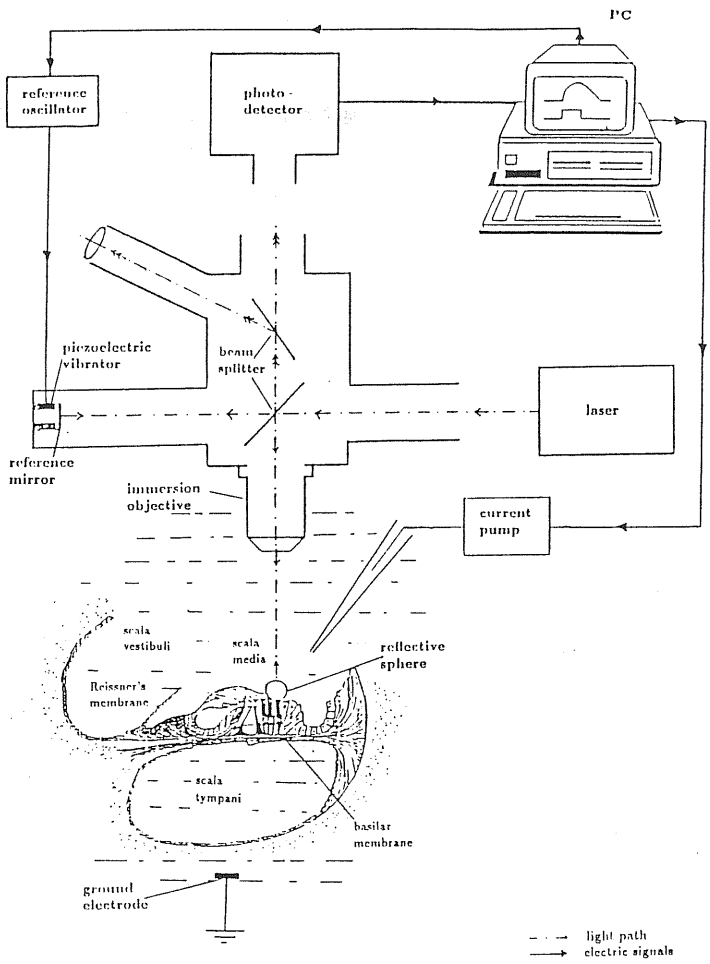

Figure 3.4: Apparatus.

a) Photograph of the Michelson interferometer incorporated in a compound microscope. Scale bar: 10 cm. The He-Ne laser and the reference mirror are attached to the microscope body, with micrometric controls for alignment. Polarising filters are used to gradate the intensity of the beams. The instrument is placed in a sound–proof enclosure, constituted by a double–walled wooden box (not shown). The 4cm space between the walls is filled with sand and the box sits over pneumatic suspensions. At present, displacements of approximately 0.1 nm (10^{-10} m) can be detected while working in a moderately noisy environment.

b) The chamber with the cochlea is seen under the objective.

c) Scheme of the apparatus. Arrow heads indicated the direction of signal transmission. The reference mirror is mounted on a piezoelectric disc. The position of the mirror is controlled with a computer by varying the potential at the element. The same computer is used for on–line analysis of the digitised photocurrent. Stimuli are produce by an isolated stimulator. When frequency analysis is performed, the photocurrent is sent to a lock–in–amplifier and stimuli are generated by a voltage–controlled oscillator.

The chamber is put under a compound microscope, coupled to a Michelson interferometer (Fig.3.4). In this instrument, a laser beam is partially reflected by a beamsplitter and directed towards the cochlear partition through the objective. The fraction of the beam that traverses the beamsplitter impinges on a reference mirror, which is mounted over a piezoelectric disc. Light reflected by a bead sitting over the cochlear partition interferes with light reflected by the mirror. The interference signal, which is detected by a photodiode, is a circular pattern of fringes formed by the plane wavefronts reflected by the reference mirror intersecting the curved wavefronts reflected by the bead. The fringe spacing depends on the distance from the focus of the objective to the bead. The displacement undergone by a bead is approximately proportional to the modulation of the photocurrent only if the photodiode is uniformly illuminated (see next section). If this is not ensured, the modulation signal will also depend on the number of fringes which project onto the photodiode. A uniform illumination over the laser beam cross–section (one–fringe condition) is obtained by matching the curvature of the impinging wavefront to that of the bead. This is accomplished by suitably placing the focus below the top of the bead.

A glass pipette with a resistance of 200–300 kΩ is inserted in the gap between the water–immersion objective (40$\times$ Zeiss WI) and the cochlea. This type of objective eliminates the disturbances that a mobile liquid interface would cause to the interference signal. The tip of the pipette is placed above the cochlear partition, approximately 200 μm from the site to be stimulated. Stimuli consist of either steps or sinusoidal potentials applied between the pipette and the silver–cloride pellet sitting at the bottom of the chamber. The photocurrent is sampled at 41666 Hz with an analog–to–digital interface (Cambridge Electronic Design model 1401) driven by a PC/386 running software written for the project. Sinusoidally varying voltages are delivered with a built–in voltage control oscillator when performing frequency analysis with a lock–in–amplifier (Stanford Research model SR530). Current flowing across the cochlear partition is measured through the voltage drop at the extremes of a 1 kΩ resistor in series with the bath. At onset and offsett of steps, 30 μs transients due to the capacitance distributed along the pipette are sometimes noticed in the current record.

Determination of cochlear partition displacements

Referring to Fig.3.4, let us define the distance from the beamsplitter to the reflective bead as x_1 and that from the beamsplitter to the reference mirror as x_2. The photocurrent is proportional to the intensity I of the recombined beam where

$$I = I_o \left[1 + \cos\left(\frac{4\pi}{\lambda}(x_1 - x_2)\right)\right]$$

where λ is the laser wavelength and I_o measures the intensity of the radiation emitted by the laser (see Appendix). Clearly, I is well approximated by a linear function over the ranges $[0, \pm\lambda/4]$. Therefore, the optimal condition for detecting changes in $x_1 - x_2$ is that of keeping the resting value of $x_1 - x_2$ (baseline) around an inflection point of I, i.e. around $\pm\lambda/8$. Under these conditions, the largest deviation from linearity occur at the extremes of these intervals, where the displacement of the bead will be underestimated by at most 13 %.

The principal difficulty which arises when trying to maintain the inflection–point condition is determined by changes of temperature of the two arms of the interferometer and/or swelling or shrinking of the organ of Corti. The instability of the baseline not only compromises the linearity of the measure, but also affects the phase of the photocurrent which depends on $x_1 - x_2$ being closer to $-\lambda/8$ or to $+\lambda/8$. As signal averaging is generally necessary, phase reversals occurring within the same averaging session are clearly disastrous. Even in the fortuitous case that the average does not vanish altogether, it would still be impossible to relate the phase of the displacement to that of the averaged photocurrent. Consequently, it would be impossible to know whether the cochlear partition moves up or down for a given polarity of the stimulus. Fluctuation of the laser intensity I_o constitute a further potential source of errors, as it is clear that the photodiode cannot discriminate between changes in $x_1 - x_2$ and changes in I_o.

These problems are solved by selecting an appropriate stimulation cycle and by dynamically controlling the position of the reference mirror. During an averaging session, approximately half of each sampling interval $[0, T]$ is used to stimulate the cochlea. At time $t_o \approx 2T/3$ the reference mirror is vibrated for a cycle of a sinewave of frequency $10/T$, at a peak–to–peak amplitude of $\lambda/4$. T is chosen such

that the photocurrent in $[t_o, T]$ is modulated solely by the symmetrical vibration of the reference mirror. The distance of the baseline of $x_1 - x_2$ from $\pm\lambda/8$ is measured by the degree of asymmetry in the photocurrent. Define S_{max} and S_{min} as the maximum and minimum of the photocurrent during the interval $[t_o, T]$, respectively.

If the ratio $|S_{max}/S_{min}|$ differs appreciably from 1, the baseline is not sitting over inflection point of the intensity function I. The whole sample is then rejected. A dc offset voltage, proportional to the drift of the baseline, is sent from the DAC in the computer interface to the piezoelectric disc over which the reference mirror is attached, via a low–pass filter. The filter serves for smoothing the voltage steps sent to the element. In this way the resting value of $x_1 - x_2$ is modified in a continuous fashion, bringing it progressively closer to $\pm\lambda/8$. As baseline drifts occur normally on the time–scale of seconds, the cutoff–frequency of the low–pass filter is set to 1 Hz.

If the sample is accepted, it is divided by S_{max} and multiplied by $\pm\lambda/8$. As the reference mirror is vibrated always in the same way, the sign is selected by determining whether S_{max} precedes or follows S_{min}. Thus, the photocurrent is recalibrated at every sampling interval. Phase reversals, as well as fluctuations of the laser intensity taking place on a time scale larger than T, are compensated for.

The relationship between the phase of the averaged photocurrent and the direction of the BM displacement relative to the microscope was assessed once for all by putting a second piezoelectric–driven mirror under the objective, instead of the cochlea.

3.4 Results

Most records were taken at sites located approximately 7 mm from the helicotrema (11 mm from the stapes). Data from specimens where the cochlear partition was suspected to have been damaged during the dissection were discarded.

Responses to pulses

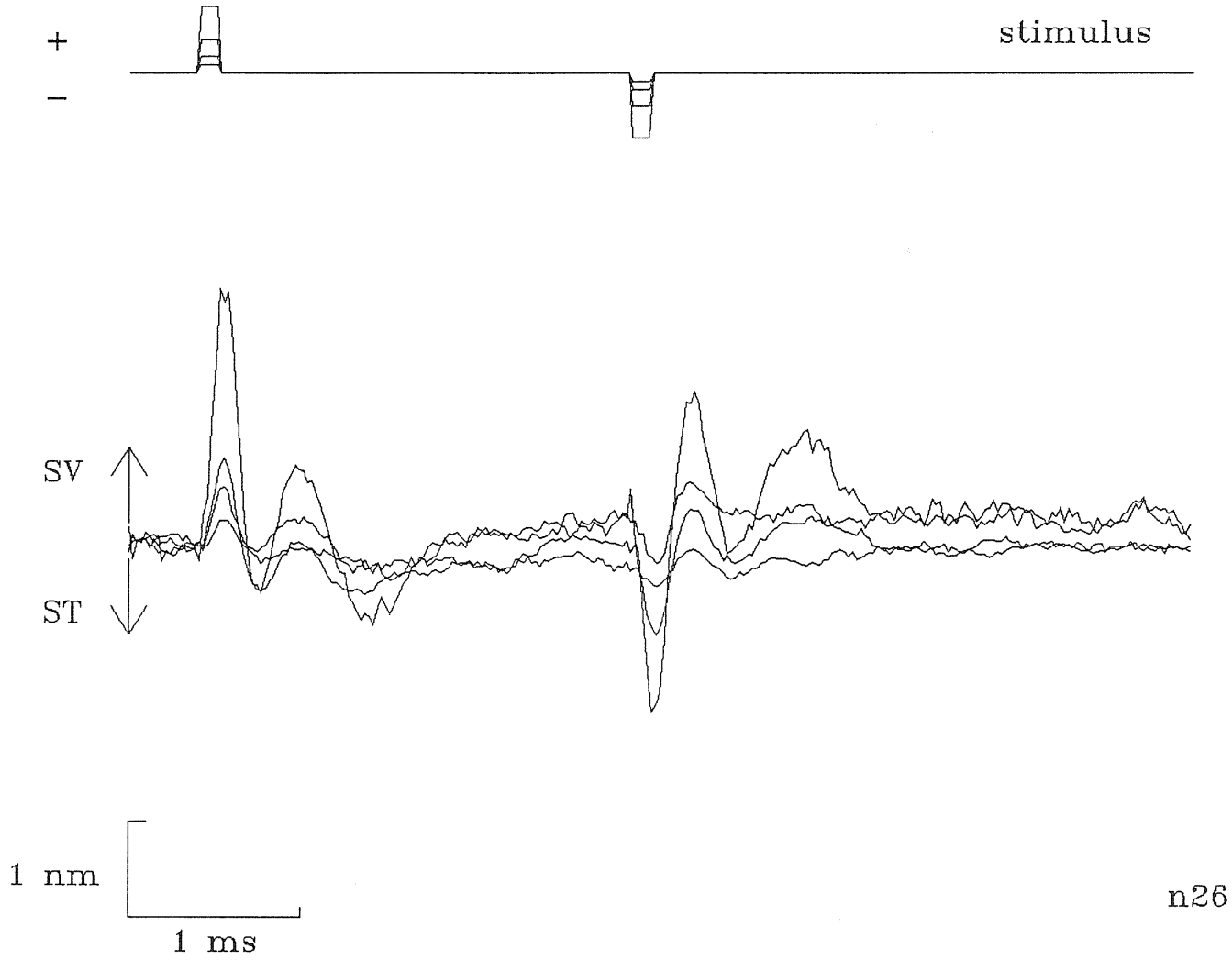

Figure 3.5: BM displacements

elicited by 100 μs pulses at current levels of 300, 150, 75, 32.5 μA. Approximate distance from the helicotrema: 7.0 mm. Averaged responses, 100×.

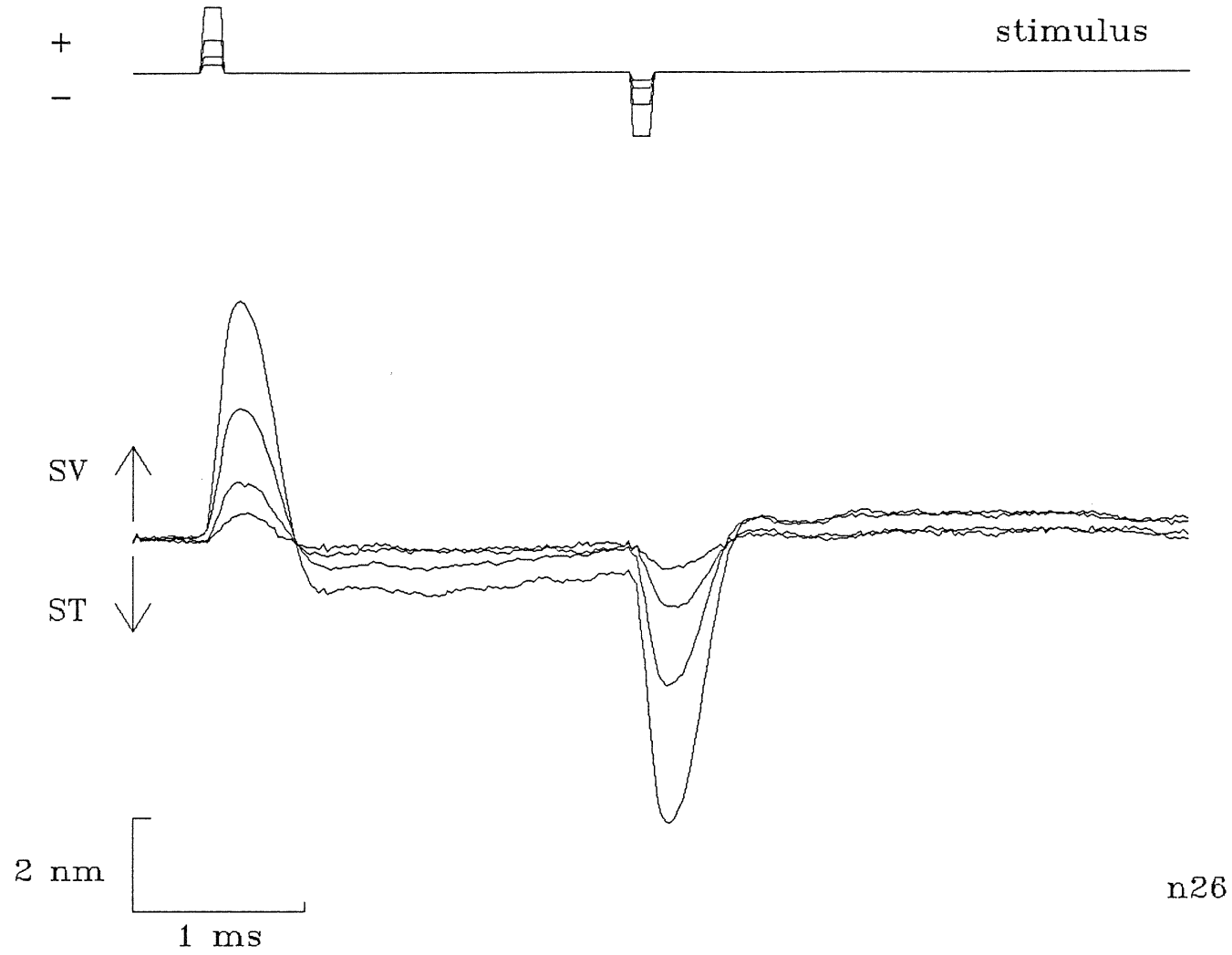

Figure 3.6: TM displacements.

Same experiment of Fig.3.5, same cochlear site and stimuli. Averaged responses, 100×.

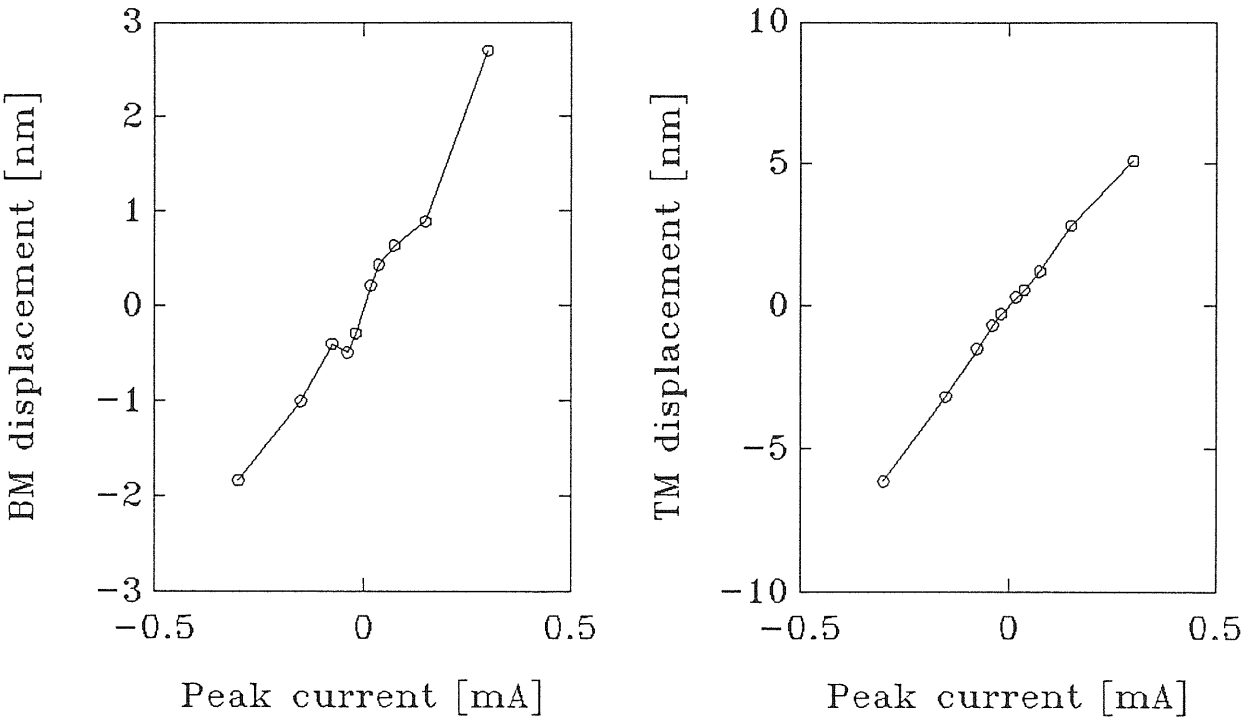

Figure 3.7: Maxima of BM and TM responses to short pulses plotted against stimulus amplitude, for the traces shown in Fig.3.5 and Fig.3.6.

The response of the BM to 100 μs pulses was a damped oscillation (Fig.3.5). The same stimuli elicited 2 to 5 times larger displacements of the TM, generally characterized by a higher degree of damping (Fig.3.6). The BM oscillated for approximately 2 cycles at frequencies about 1.8 kHz. The TM oscillated for at most 1 cycle at frequencies about 1 kHz, or simply returned to the baseline after peaking only once. BM and TM responses increased linearly with current in the range from 20 to 300 μA (Fig.3.7).

Responses to steps

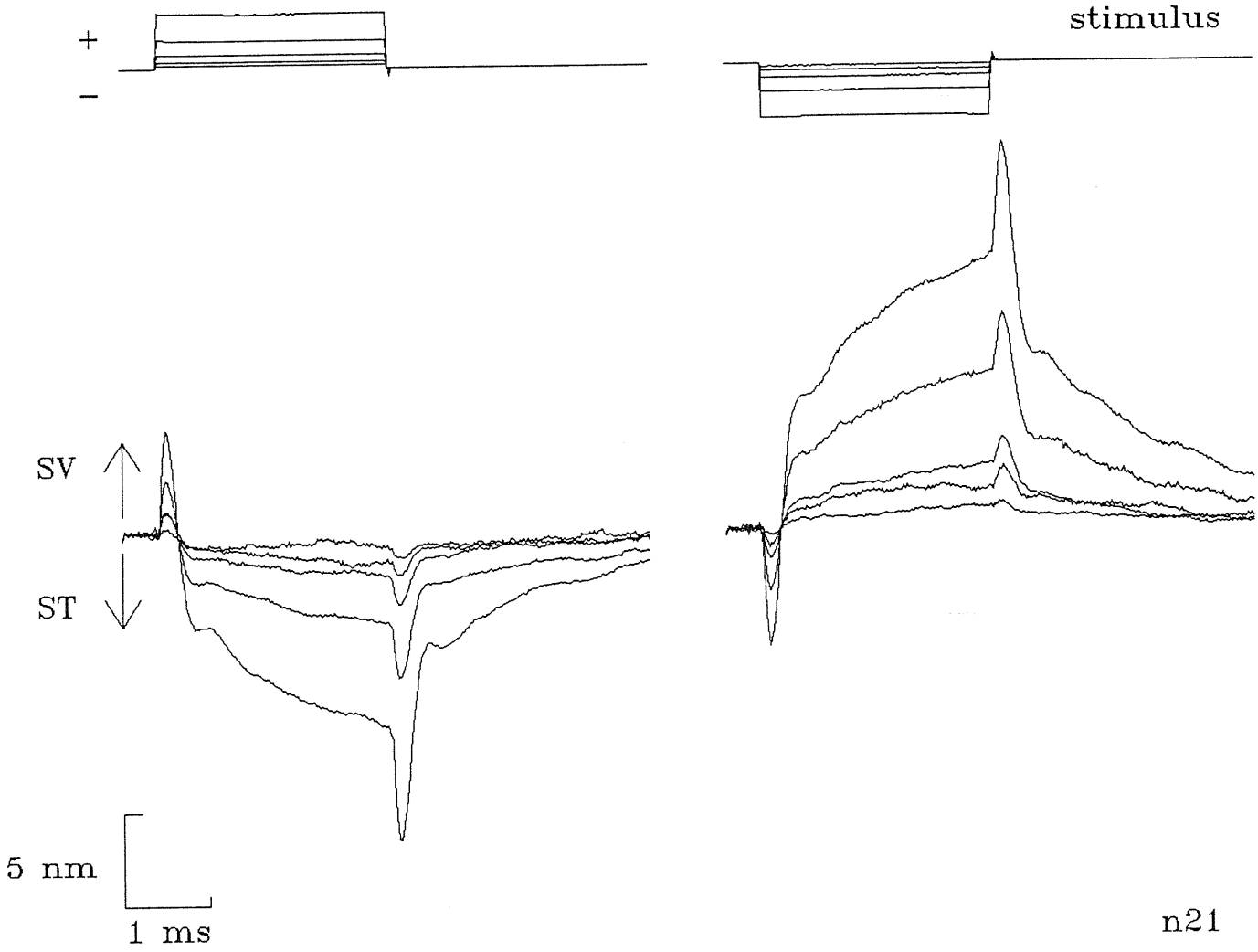

Figure 3.8: BM displacements

elicited by steps at current levels of 320, 160, 80, 40, 20 μA. Approximate distance from the helicotrema: 7.0 mm. Averaged responses, 100×.

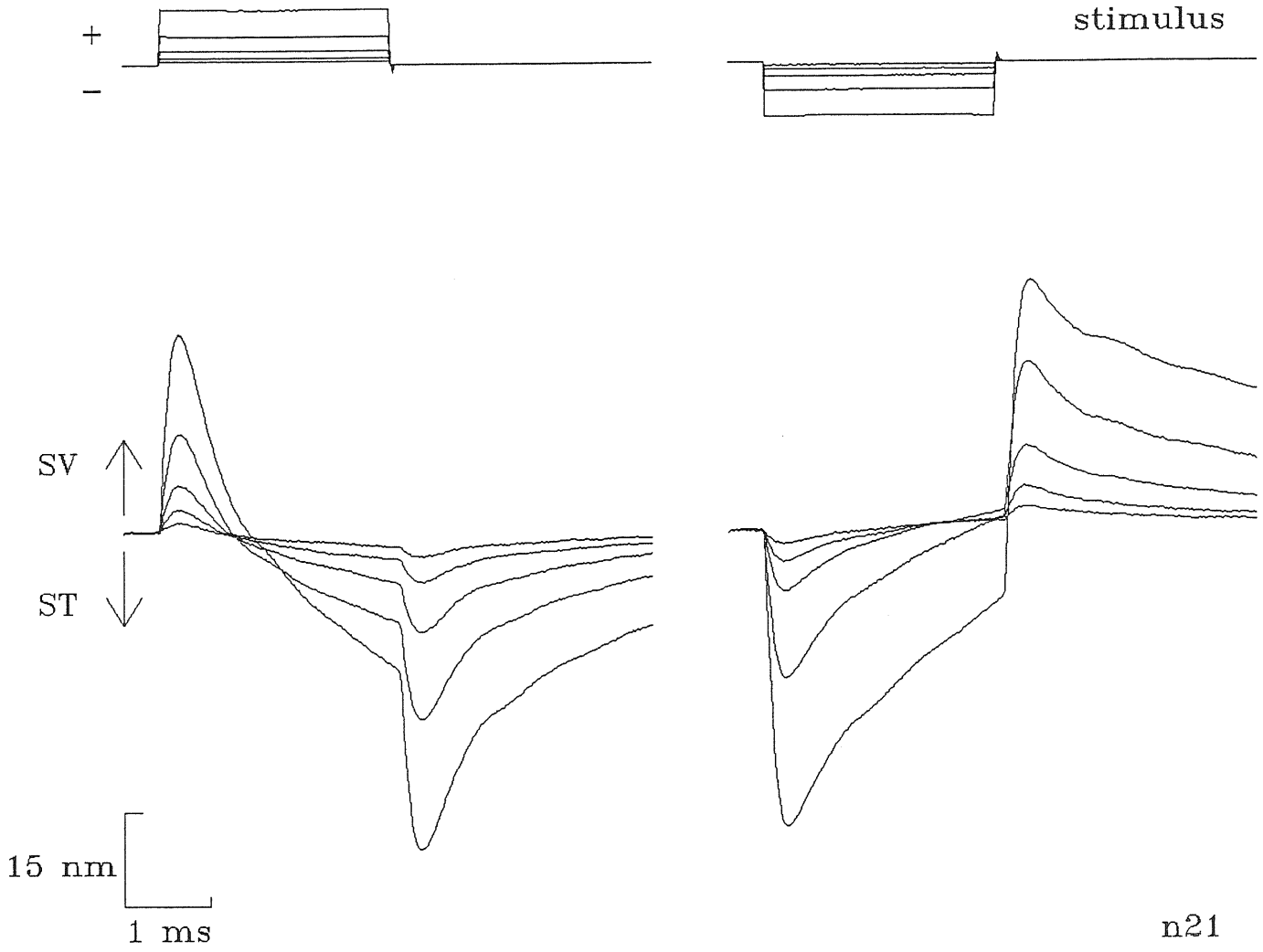

Figure 3.9: TM displacements.

Same experiment of Fig.3.8, same cochlear site and stimuli. Averaged responses, 100×.

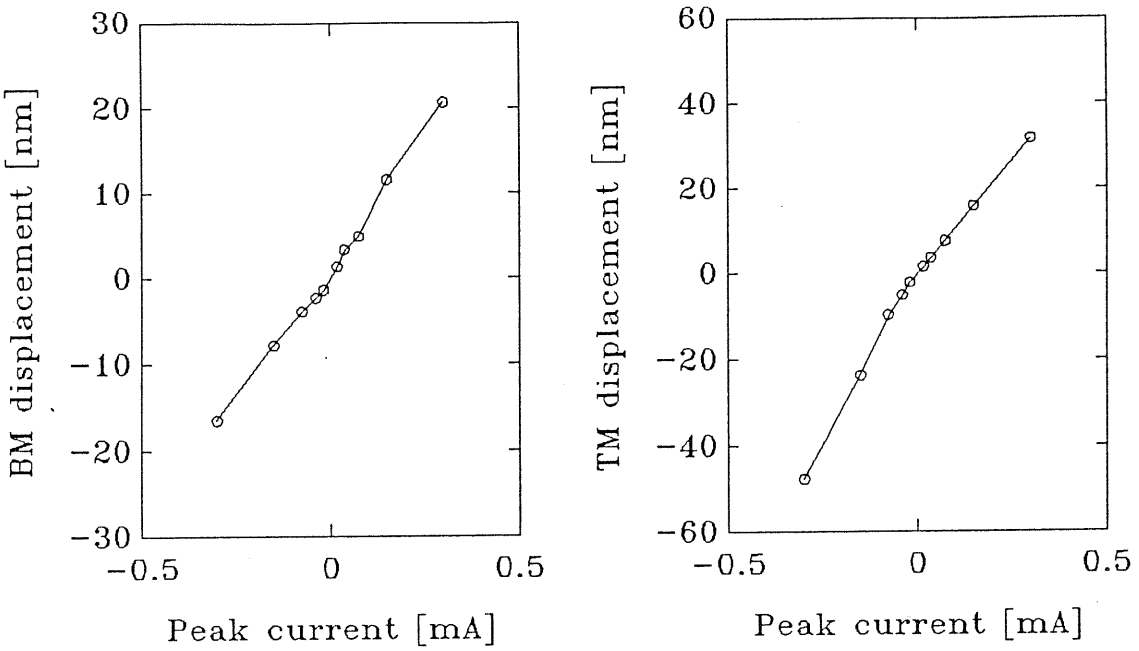

Figure 3.10: Maxima of BM and TM responses to steps plotted against stimulus amplitude, for the traces shown in Fig.3.8 and Fig.3.9.

At onset of long command steps the BM responded with a rapid oscillatory transient lasting 200-400 μs. The displacements then grew in the direction opposite to the initial one. At offset, again the BM responded with a transient and slowly returned to the baseline. Small oscillations were often noticeable during the post–transient tracts. The polarity of the step influenced the magnitude of the responses, in that displacements in the direction of scala vestibuli were consistently larger than those in the opposite direction. Fig.3.8 shows a representative response pattern.

The responses of the TM showed a larger variability form specimen to specimen. In general, they were slower than their BM counterparts and often no oscillatory transient could be seen. The variability concerned the degree of asymmetry in the responses elicited by opposite polarities of the pulses. A particularly asymmetric response is illustrated in Fig.3.9. A preference for displacements towards scala tympany is noticeable. With TM responses of the more symmetric type, the BM and the TM moved generally in phase for approximately 120–130 μsec and in antiphase for the remainder of the command step. In every circumstance, TM displacements were 3–5 times larger than BM ones. BM and TM responses increased linearly with current from 20 to 300 μA (Fig.3.10).

Time evolution and frequency analysis of BM responses

Figure 3.11: Time course of the BM response to steps.
Current level: 310 μA. Numbers at the left of each trace give time from dissection.

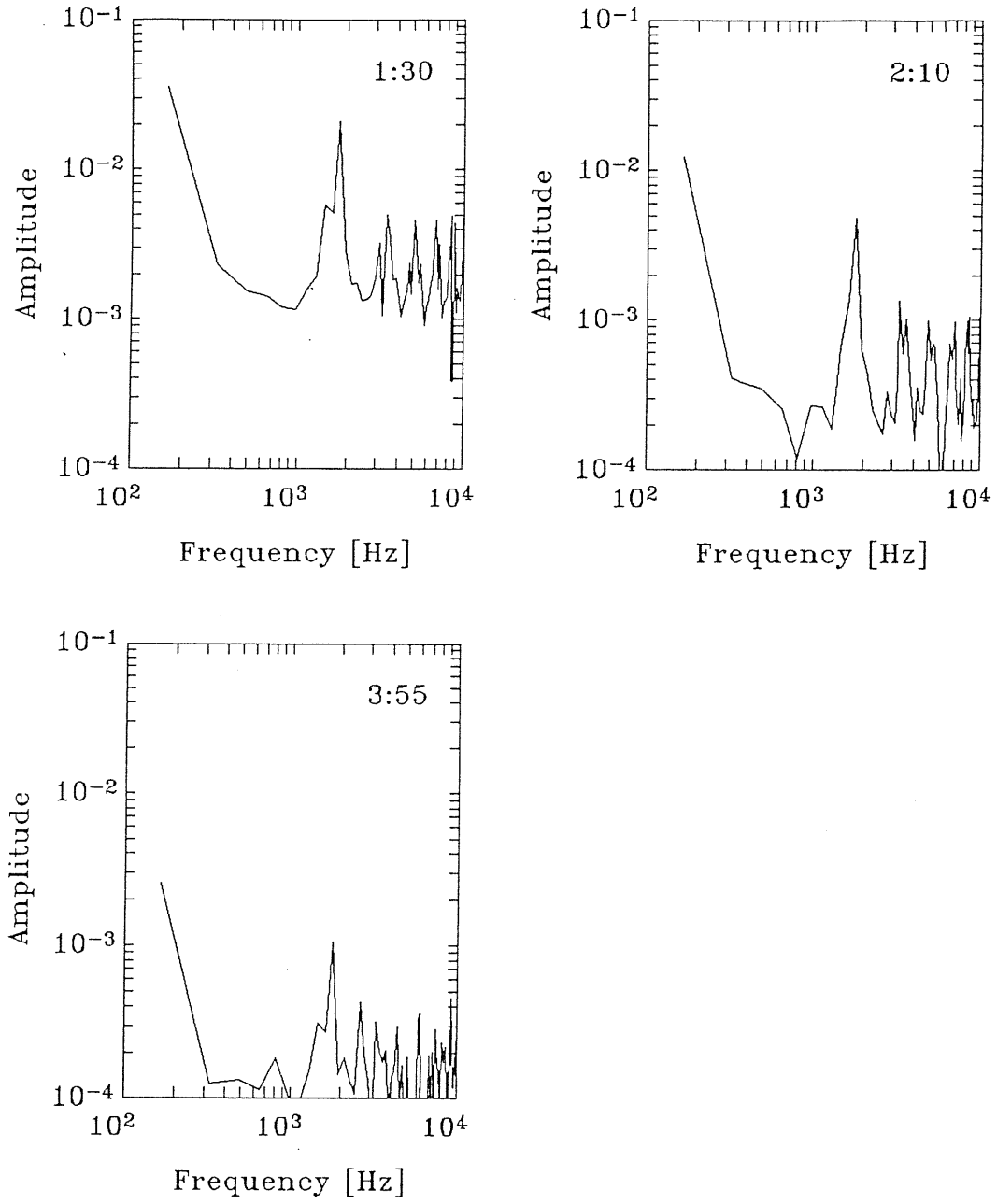

Figure 3.12: Time course of the BM transfer function estimated from the traces shown in Fig.3.11. Ordinates give the transfer function magnitude in arbitrary units. Numbers at the upper right corner of each inset give time from dissection.

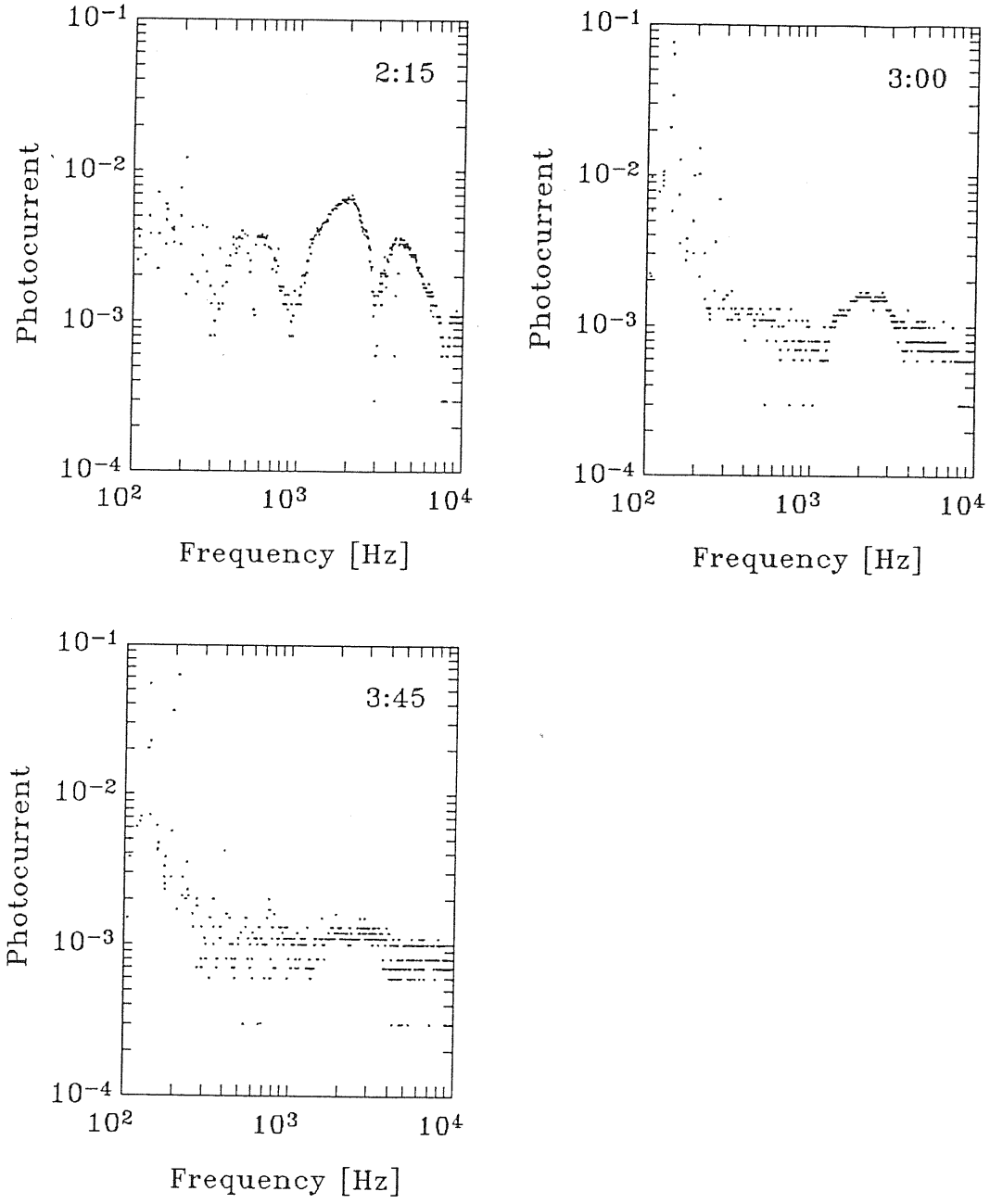

Figure 3.13: Time course of the BM frequency response,
as assessed with a lock–in–amplifier. Stimuli were sinewaves in the shown frequency range at 500 μA peak–to–peak current level. Ordinates give magnitude of the photocurrent in arbitrary units. Numbers at the upper right corner of each inset give time from dissection.

The responses were maintained generally for three to six hours and declined thereafter. On one occasion it was possible to record responses to steps and to sinusoidal stimuli from the same specimen, at a site located approximately 7.2 mm from the helicotrema (10.8 mm from the stapes). This was accomplished by alternating between the two available instrumental configurations, i.e. between time–averaging and the lock–in–amplifier. With the second configuration, the voltage–controlled oscillator built in the lock–in–amplifier was used to apply sinusoidal potentials at frequencies ranging from 50 to 10000 Hz. The amplifier measured the amplitude of the photocurrent in a narrow frequency band around the frequency of the stimulus.

Fig.3.11 illustrates the decline with time of the BM response to command pulses during the aforementioned experiment. The BM *transfer function* is estimated from each of the traces in Fig.3.12 by dividing the Fourier transform of the time responses by the transform of the stimulus. Fig.3.13 illustrates the result of frequency analysis performed on the same specimen with the lock–in–amplifier. Both methods show a resonant peak at approximately 1.8 kHz, and other peaks at the harmonics of this frequency.

3.5 Discussion

According to the most recent determination of the guinea pig frequency map (Greenwood, 1990), the characteristic frequency of the cochlear site located 7mm from the helicotrema is 2 kHz. The map varies at a rate of approximately 2.3 mm/octave. These data refer to living animals. In the basal turn of the cochlea the resonance frequency of the BM shifts back by approximately half an octave and the sharpness of the resonance drops dramatically *post mortem* (Sellick *et. al.*, 1982).

The series of experiments presented here shows that, in the proximity of the 7 mm site, damped resonating oscillation of the BM, at frequencies comprised between 1.5 and 1.8 kHz are elicited by extracellular current. These frequency values are compatible with the expected half–octave–shifted characteristic frequency of this site. The quality factor of the responses varies between 1.2 and 2. Considering that the results come from dead specimens, this compares well with the values 2–4 of the Q_{10} from neural data *in vivo* at the same site (Evans, 1975).

The results show that the TM is displaced 2 to 5 times more but oscillates less than the BM at the same site, giving highly–damped responses. As the triggering of the sensory receptors in the organ of Corti relies on the shear displacement between the reticular lamina and the TM, differences in the vibration patterns of the TM and the BM are expected. The higher degree of damping shown by the TM may result from the viscosity of the fluid in the narrow cleft separating the TM from the reticular lamina.

This study was motivated by the need to clarify the role of outer hair cells in mammalian hearing, aiming in particular, at answering the question whether these cells form the cellular basis of the "cochlear amplifier". In this respect, it is interesting to note that Hubbard and Mountain (1983) elicited sound pressure changes in the external meatus as a consequence of current injection in the scala media of anesthetised animals. The sound spectrum generated by the injection of sinusoidal current presented components at the electrical frequency and its harmonics. The current levels they used were comparable to those used in the experiments reported here. Hubbard and Mountain claimed that current was exciting the sound transduction chain backwards, with the outer hair cells exerting forces over the cochlear partition, and that these forces were transmitted to the tympanic membrane by the cochlear fluid. The main argument in favour of the hair cells was the lability of the response.

The results shown here substantiate Hubbard and Mountain's data, in that current does indeed produce measurable mechanical responses of the cochlear partition. The responses are labile and are characterized by spectral peaks at the half–octave–shifted characteristic frequency of the site and its harmonics. In an intact cochlea, these responses would undoubtedly propagate their action to the stapes through the cochlear fluid, generating sound. Furthermore, the responses to command pulses are different for the BM and the TM. In particular, after the oscillatory transients of the BM die out, the BM and the TM tend to move in antiphase. This indicates that the cochlear partition changes its shape, as expected if current is eliciting motile responses in the outer hair cells (Fig.2.4).

Appendix: fundamentals of laser interferometry

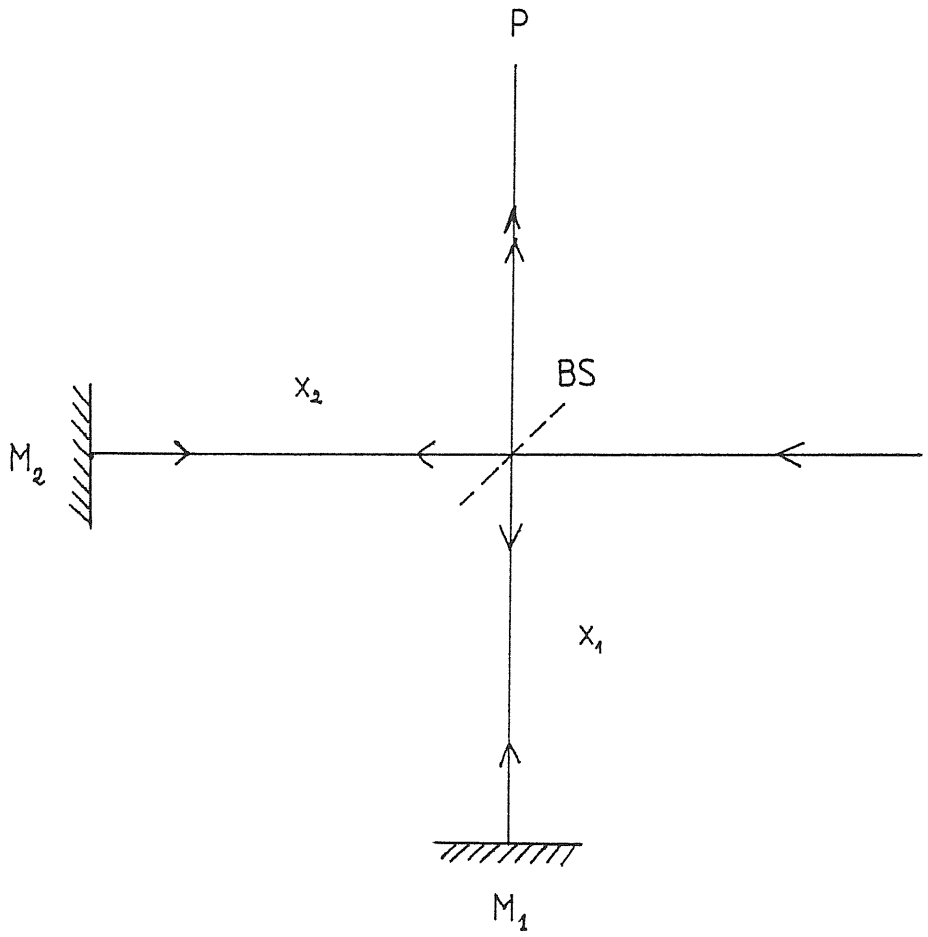

Figure 3.14: Scheme of a Michelson interferometer.

Laser interferometry constitutes the preferred framework for the detection of atomic–scale displacements. The scheme of a Michelson interferometer (Michelson, 1882) is shown in Fig.3.14.

Let $E_1 = A_1 \exp[i(\omega t + \phi_1)]$ and $E_2 = A_2 \exp[i(\omega t + \phi_2)]$ be the complex representation of the electric–field components of the laser beams interfering at P. ω is the angular frequency of the laser light, t is time, A_1 and A_2 the (real) amplitudes of the fields. The phase difference, caused by the different retardation suffered by the two beams resulting from the propagation from BS to M_1 and from BS to M_2 is

$$\phi_1 - \phi_2 = \frac{2\pi}{\lambda}(2x_1 - 2x_2),$$

Radiation at P can be measured a by photodiode, i.e. a semiconductor device in which light is detected by the production of electron–hole pairs in the junction region of a p–n diode. If the diode is reverse–biased, current does not pass owing to the junction region being depleted of charge carriers. However, illumination by light of appropriate wavelength–range generates electrons and hole carriers which are drawn by the electric field in the junction to the n and p sites, respectively, before they can recombine. This produces a measurable leakage current (photocurrent). The fastest photodiodes sensitive to optical radiation have a response time of about 10^{-10} sec. During that time interval there will be about 10^5 oscillations of the recombined electric field $E_1 + E_2$. The photodiode will thus be able to respond only to the average intensity

$$I \equiv < (E_1 + E_2)^2 > \equiv \frac{1}{T}\int_{t-T/2}^{t+T/2}(E_1 + E_2)^2\, dt,$$

where T is the photodiode response time. Expanding and averaging we find

$$I = \frac{1}{2}(A_1^2 + A_2^2) + A_1 A_2 \cos\left[\frac{4\pi}{\lambda}(x_1 - x_2)\right].$$

If $A_1 = A_2$ this expression simplifies to

$$I = I_o\left[1 + \cos\left(\frac{4\pi}{\lambda}(x_1 - x_2)\right)\right]$$

where $I_o = 2A_1^2$. The cosine term represents the actual interference product and is the one from which the information relative to the state of the paths x_1 and x_2 can be extracted. Clearly, if any one of the mirror is displaced, the path difference above will change, which will in turn alter the intensity I at P and will be detected as a modulation of the photocurrent amplitude.

Notice that maxima of the intensity function I are found at $x_1 - x_2 = 2n\,\lambda/4$, $n = 0, 1, 2\ldots$ (constructive interference), whereas minima are found at $x_1 - x_2 = (2n+1)\,\lambda/4$, $n = 0, 1, 2\ldots$ (destructive interference). As I is periodic, the largest displacement that a Michelson interferometer can measure (without counting the number of times a maximum or a minimum is crossed) corresponds to $\lambda/4$. For an ordinary He-Ne laser this is approximately 80 nm.

Chapter 4

The cochlea as a formant detector

4.1 Abstract

Rather than simply analysing the spectral composition of sounds, the cochlea of higher vertebrates seems optimised for detecting *formants*, i.e. the resonance characteristics of sound sources. It is thought that the motile properties of the outer hair cells are responsible for the sharp frequency selectivity and speed of response of the cochlea and that the ability of humans to use speech relies on the correct functioning of these cells. In this chapter the results of computer–simulated speech filtering performed by a cochlea with and without contributions from the outer hair cells are compared. It is shown that linear active processes, compatible with the physiology of the outer hair cells, can indeed improve the detection of high–frequency formants. The detection of low–frequency formants requires also the intervention of nonlinear processes.

4.2 Speech–feature detection in the cochlea

Speech is generated by the excitation and modulation of the vocal tract. This is a bifurcating cavity terminated on one end by the glottis and on the other by the mouth and nose orifices. *Voiced sounds* are produced by exciting the vocal tract with quasi–periodic pulses of air flow caused by vibration of the vocal cords.

The frequency of vibration of the vocal cords is called *pitch* (F_0). In humans, F_0 normally ranges from 100 Hz (males) to 300 Hz (females). The features of voiced sound are determined by the acoustical transfer properties of the vocal tract or, more specifically, by its resonance frequencies, also called *formants.* In normal speech, there are three perceptually relevant formants: F_1 (270–730 Hz, m.; 310–860 Hz, f.) F_2 (840–2290 Hz, m.; 920–2790 Hz, f.) F_3 (1690–3010 Hz, m.; 1960–3310 Hz, f.; data after Peterson and Barney, 1952).

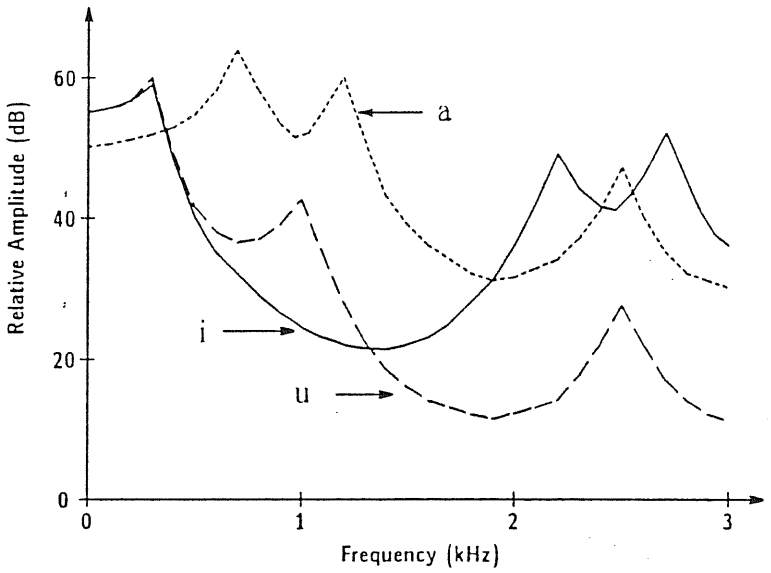

Figure 4.1: Cross section of spectra
from the middle of English vowels, for a male speaker, showing formants as spectral peaks. From O'Shaughnessy (1990), Fig.3.11.

In Fourier analysis, a formant is represented as a complex–plane pole with frequency for real part and damping constant for imaginary part. The Fourier spectrum of a voiced sound is the superposition of the pitch harmonics, modulated both in amplitude and phase in a way that depends upon the location of the formants on the complex plane (Fig.4.1). When emitting speech, the vocal tract changes shape on a time base of approximately 10 ms. The position of the formants on the complex plane varies continuosly as the resonance characteristic of the vocal tract change. Since formants convey all the acoustical information necessary to distinguish a phoneme, the understanding of speech relies of the ability of the auditory system to track the evolution of formants.

The cochlear filter seems capable of sorting out the formant structure of speech before further information processing takes place. The activity of the acoustic nerve maps *tonotopically* the vibration of the cochlear partition. This is to mean that each *afferent* nerve fibre is excited maximally by the frequency that makes the travelling wave (TW) peak at the site of the basilar membrane (BM) where that fibre contacts the *inner* hair cells within the organ of Corti. High frequencies peak near the stapes, low frequencies near the helicotrema. The frequency which maximises the response of a fiber is called *characteristic frequency* (CF) of the fibre.

The firing pattern elicited by simple speech–like sound has been extensively studied in the cat. Secker–Walker and Searle (1990) showed that these sounds selectively trigger those fibres of the acoustic nerve which possess a CF near F_0, F_1, F_2, F_3 (Fig.4.2). It is thought that this is achieved through the intervention of the *outer* hair cells (OHCs) in the mechanical control of the vibration pattern of the BM (Pickles, 1988). In this chapter, results of a mathematical analysis of cochlear dynamics previously illustrated are applied to investigate the speech–filtering capabilities of the human cochlea.

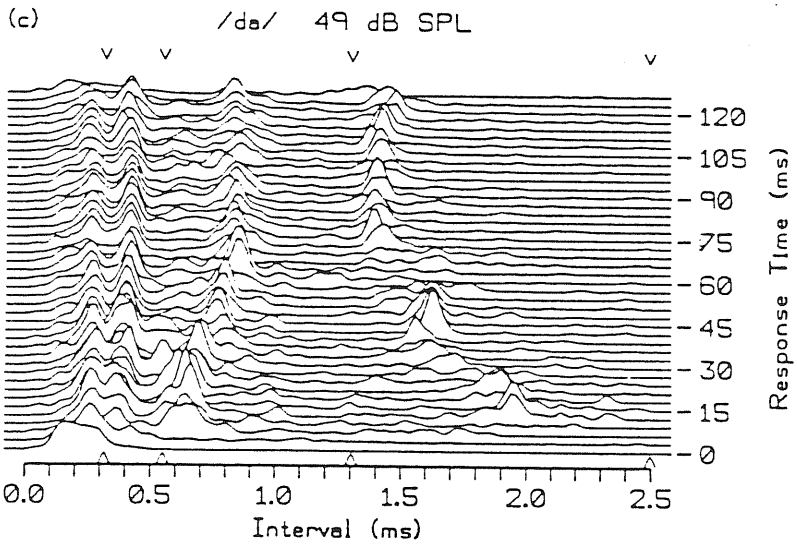

Figure 4.2: Response of the auditory nerve to sound.
Pooled interpeak interval histogram of the response to /da/. Arrowheads mark boundaries between interval bands used in formant estimation. From Secker–Walker and Searle (1990), Fig.6.

4.3 Formant detection in the linear approximation

In Chapter 2 it was shown that the solutions $\tilde{\xi}(\omega, x)$, of the integral equation 2.16 (reported here for the sake of clarity)

$$\int_0^1 H_\omega(x, \bar{x};\, \lambda)\, \tilde{\xi}(\omega, \bar{x}) d\bar{x} \;=\; \omega^2 G_S(x)\, \tilde{\sigma}(\omega)\,,$$

reproduce rather realistically the responses of the BM to pure tones. Parameter $\lambda \in [0, 1]$ represents the degree of efficiency of the OHCs. As λ approaches 0, the OHCs compensate less the dissipative losses due to viscosity (passive cochlea). Correspondingly, broadly tuned solutions are generated, which resemble closely the TWs observed by von Bèkèsy in cadavers (Fig.2.3). As λ approaches 1, OHC motility tends to cancel the dissipative losses almost completely, and the solutions of the above equation become sharply tuned (Fig.2.5).

Two sets of solutions for the passive and active case can be obtained, in the frequency domain, by solving the above equation numerically for a large enough set of harmonics ($\omega = n\,\omega_o$; $n = 1, 2, 3, \ldots$). This is accomplished by approximating the integral kernel with an $N \times N$ matrix $\mathbf{H}(\omega)$ the elements of which are the the values of $H_\omega(x, \bar{x};\, \lambda)$ computed on a discrete mesh in the unit square $[0\,, 1] \times [0\,, 1]$. Performing the inversion of this matrix in the two cases ($\lambda \rightarrow 0$) and ($\lambda \rightarrow 1$) yields the two sets of vector solutions

$$\vec{\xi}_n^{\,0} = (n\,\omega_o)^2\, \mathbf{H}^{-1}_{\lambda \rightarrow 0}(n\,\omega_o)\, \vec{G}_s$$

and

$$\vec{\xi}_n^{\,1} = (n\,\omega_o)^2\, \mathbf{H}^{-1}_{\lambda \rightarrow 1}(n\,\omega_o)\, \vec{G}_s$$

where $\vec{G}_s$ is the propagator $G_S(x)$ evaluated at the border of the mesh.

In the linear approximation, the response of either the passive or the active BM to an external signal of period $T = 2\pi/\omega_o$ can be easily computed (in the time domain) as superposition of these solutions. We can represent the stapes displacement elicited by a quasi–periodic complex signal (like a vowel) as

$$\sigma(t) = \mathrm{Re}\left[\sum_n z_n\, \exp(i\, n\, \omega_o t)\right]\,,$$

where $i = \sqrt{-1}$, t is time and z_n are complex coefficients which depend upon the resonance characteristics of the sound source. The time–dependent BM response to this type of excitation at the stapes is then

$$\vec{\xi}^{j}(t) = \mathrm{Re}\left[\sum_n \vec{\xi}_n^{j} z_n \exp(i n \omega_o t)\right] ,$$

where superscript $j = 0, 1$ for the passive and active cochlea, respectively.

In Fig.4.1 the responses elicited by a periodic sequence of sharp gaussian spikes, simulating pitch, are shown for both passive and active regimes.

Fig.4.2 illustrates analogous responses elicited by the pitch spikes convoluted with a transfer function that simulates three cascaded cavities resonating at frequencies corresponding to average values for the formants of the /i/ vowel. These cavities are interposed between the pitch source and the auditory system to simulate the vocal tract.

The choice of /i/ was dictated by the peculiar distribution of its formants, $F2$ and $F3$ being close to each other in a distal high frequency region, whereas $F1$ is found in the low–frequency zone, in the proximity of the pitch. This will help to clarify the limits of a linear approach.

4.2 Discussion

These simulations of BM responses to vowel–like stimuli show that two narrow peaks form on a BM site corresponding to the high–frequency formants $F2$ and $F3$ only for $\lambda \rightarrow 1$, i.e. when OHC motility is included. A linear model like this seems sufficient to explain formant detection at high frequencies.

The breakdown of the model occurs at low frequencies, where an harmonic structure appears in place of $F1$, in contrast with the findings of Secker–Walker and Searle. It is interesting to note that these limits are bound to emerge *whenever* both the linearity of the underlying dynamics and a good frequency resolution are assumed, *independently of the particular representation of the cochlea.* We are bound to conclude that the detection of low–frequency formants relies upon *nonlinear* processing of sound within the cochlea. With increasing sound pressure

widths while the steep high–frequency behaviour remains unchanged (Johnstone *et al.*, 1986). Which *nonlinear* effects should then be assumed in order for formant peaks to be elicited in place of harmonic peaks? This is a challenging question which deserves attention (Mammano, 1990) particularly in view of its technological implications.

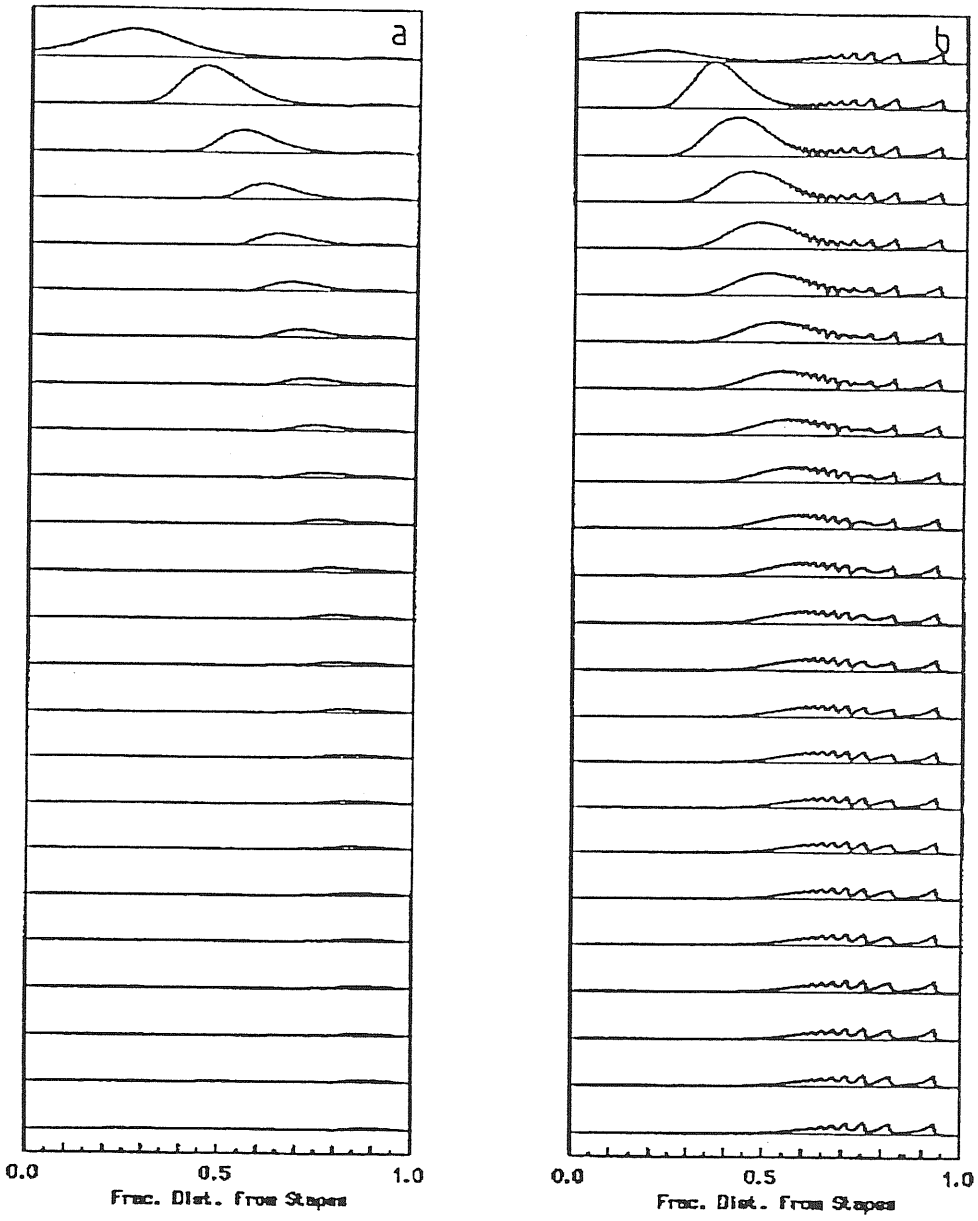

Figure 4.3: Diagrams of pitch effects

on passive– (a) and active– (b) vibration pattern of the basilar membrane, during one complete cycle of stimulation. Solutions were computed on 300 equally spaced points. Each window corresponds to a snapshot of the membrane. Intervals between frames correspond to 1/24 of a cycle. Time increases downwards. High frequencies map onto basilar membrane sites in the proximity of the stapes.

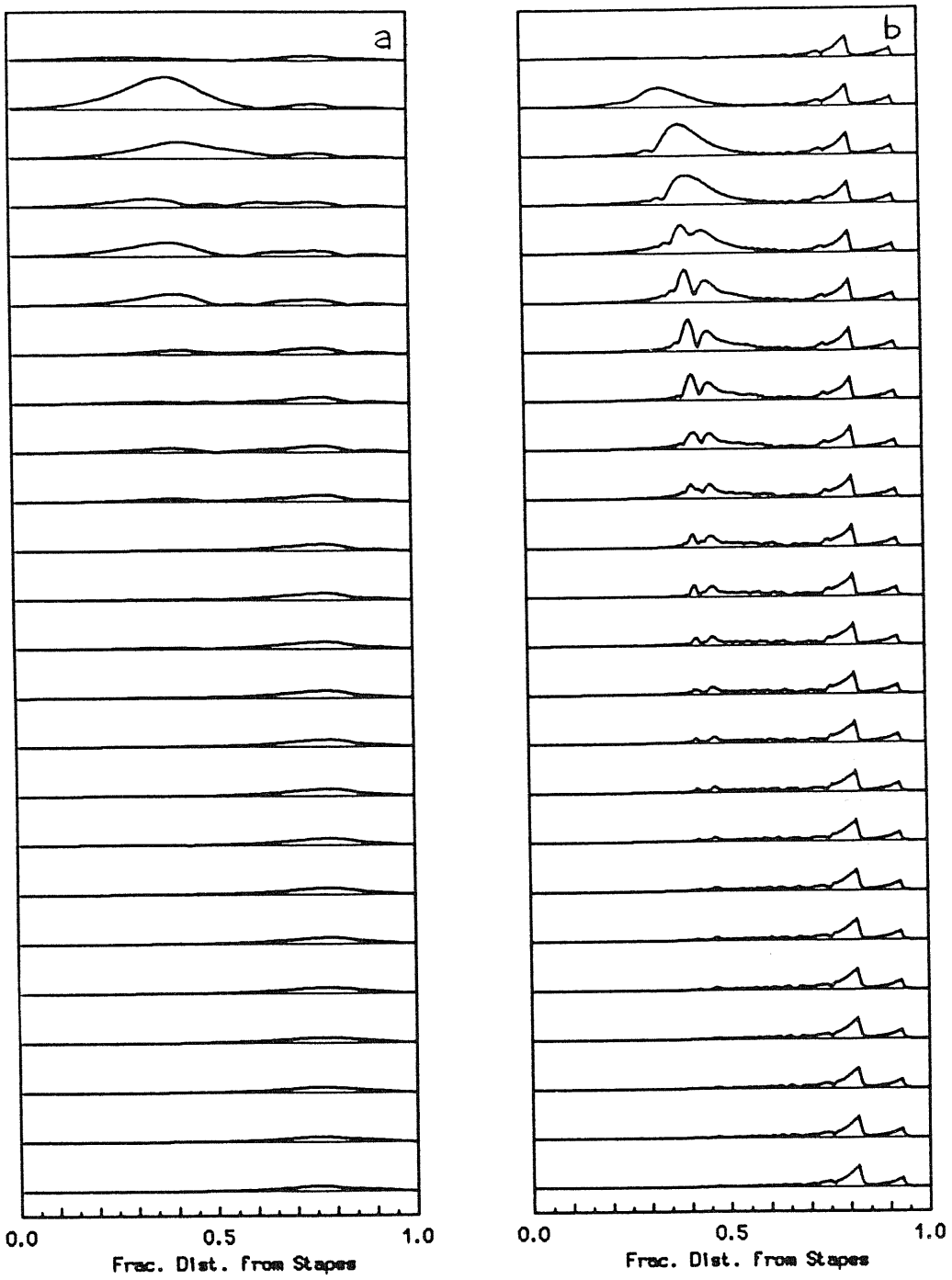

Figure 4.4: Response patterns to vowel /i/

for passive– (a) and active– (b) basilar membrane during one complete cycle of stimulation. Time course as in Fig.4.3.

Bibliography

[1] J.B. Allen, (**1977**), "Two–dimensional cochlear fluid model: New results", *J. Acoust. Soc. Am.*, **61**, 110–119.

[2] C. Angelborg and H. Engstrom, (**1973**), "The normal organ of Corti", in *Basic Mechanisms in Hearing*, A. Moller Ed., Academic Press, London, pp 125–183.

[3] J.F. Ashmore, (**1987**), "A fast motile response in guinea–pig outer hair cells: the cellular basis of the cochlear amplifier", *J. Physiol.*, *388*, 323–347.

[4] J.F. Ashmore, (**1990**), "Forward and reverse transduction in the mammalian cochlea", *Neurosc. Res.*, Suppl. 12, S39–S50.

[5] J.F. Ashmore and G.D. Housley (**1989**), "Graded ionic properties of isolated outer hair cells from the guinea–pig cochlea", *J. Physiol.*, **417**, 83P.

[6] G. von Békésy, (**1960**), *Experiments in Hearing*, McGraw–Hill.

[7] W.E. Brownell and B. Kachar, (**1985**), "Outer hair cell motility: a possible electro–kinetic mechanisim", in *Peripheral Auditory Mechanisms*, Springer–Verlag, pp 369–376.

[8] W.E. Brownell, C.R. Bader, D. Bertrand and Y. de Ripaubierre, (**1985**), "Evoked mechanical responses of isolated cochlear hair cells", *Science*, **227**, 194–196.

[9] L.M. Cabezudo, (**1978**), "The ultrastructure of the basilar membrane in the cat", *Acta Otolaryngol.*, **86**, 160–175.

[10] A.R. Cody and I.J. Russel, (**1987**), "The response of hair cells in the basal turn of the guinea pig cochlea to tones", *J. Physiol.*, **383**, 551–569.

[11] P. Dallos, (**1985**), "Response characteristics of mammalian cochlear hair cells[1]", *J. Neuroscience*, **5**, 1591-1603.

[12] P. Dallos (**1988**), "Cochlear neurobiology: some key experiments and concepts of the past two decades", in *Auditory Function: Neurobiological Bases of Hearing*, G.M. Edelman, W.E. Gall and W.M. Cowan (Eds.), John Wiley and Sons, New York, 153–188.

[13] P. Dallos, B.N. Evans and R. Hallworth, (**1991**), "Nature of the motor element in elekrokinetic shape changes of cochlear outer hair cells", *Nature*, **350**, 155–157.

[14] H. Davis, (**1958**), "Transmission and transduction in the cochlea", *Laryngoscope*, **68**, 359–382.

[15] E. de Boer, (**1980**), "Auditory physics. Physical principles in hearing theory. I ", *Phys. Rep.*, **62**, 87–174.

[16] E. de Boer, (**1984**), "Auditory physics. Physical principles in hearing theory. II ", *Phys. Rep.*, **105**, 141–226.

[17] E. de Boer, (**1991**), "Auditory physics. Physical principles in hearing theory. III ", *Phys. Rep.*, **203**/3, 125–231.

[18] E.F. Evans, (**1975**), "Cochlear nerve and cochlear nucleus", in *Handbook of Sensory Physiology*, W.D. Keidel and W.D. Neff Eds., Vol 5/2, pp 1–108, Springer, Berlin.

[19] T. Gold, (**1948**), "Hearing. II. The physical basis of the action of the cochlea", **135**, 492–498.

[20] D.D. Grenwood, (**1990**), "A cochlear frequency–position function for several species—29 years later", *J. Acoust. Soc. Am.*, **87**, 2592–2605.

[21] A.W. Gummer, B.M. Johnston and N.J. Armstrong, (**1981**), "Direct measurement of basilar membrane stiffness in the guinea pig", *J. Acoust. Soc. Am.*, **70**, 1298–1309.

[22] Y. Harada, (**1983**), *Atlas of the Ear by Scanning Electron Microscopy*, MTP Press Ltd., Lancaster.

[23] H.T.W. Helmholtz, (**1863**), *Die Lehre von den Tonempfindungen als Physiologische Grundlage fur die Theorie der Musik*, 1st ed., Brunswick, Germany, Vieveg–Verlag.

[24] M.C. Holley and J.F. Ashmore, (**1988**), "A cytoskeletal spring in cochlear outer hair cells", *Nature*, **335**, No. 6191, 635–637.

[25] A.E. Hubbard and D.C. Mountain, (**1983**), "Alternating current delivered into the scala media alters sound pressure at the eardrum", *Science*, **222**, 510–512.

[26] S. Iurato, (**1961**), "Submicroscopic structure of the membranous labyrinth. 2. The epithelium of Corti's organ", *Z. Zellforsh.*, **53**, 259–298.

[27] S. Iurato, (**1962**), "Functional implications of the nature and submicroscopic structure of the tectorial and basilar membranes", *J. Acoust. Soc. Am.*, **62**, 1386–1395.

[28] B.M. Johnstone, R. Patuzzi and G.K. Yates, (**1986**), "Basilar membrane measurements and the travelling wave", *Hear. Res.*, **22**, 147–153.

[29] D.T. Kemp, (**1978**), "Stimulated acoustic emission from within the human auditory system", *J. Acoust. Soc. Am.*, **64**, 1386–1391.

[30] N.Y.S. Kiang, E.C. Molston and R.A. Levine, (**1970**), "Auditory nerve activity in cats with normal and abnormal cochleas", in *Sensorineural Hearing Loss*, G.E.W. Wolstenholme and J. Knight (Eds.), 241–268, CIBA Foundation Symposium. Churchill, London.

[31] D.O. Kim, (**1984**), "Functional roles of the inner– and outer–hair–cells subsystems in the cochlea and brainstem", *Hearing Science*, 241–262, C. Berlin Ed., College–Hill Press, S.Diego, CA.

[32] P.J. Kolston, (**1988**), "Sharp mechanical tuning in a cochlear model without negative damping", *J. Acoust. Soc. Am.*, **83**, 1481–1487.

[33] D.J. Lim, (**1986**), "Functional structure of the organ of Corti: a review", *Hear. Res.*, **22**, 117–146.

[34] F. Mammano, (**1990**), "Modelling auditory system nonlinearities through Volterra series", *Biol. Cyb.*, **63** (4), 307–313.

[35] A.A Michelson, (**1882**), *Phil. Mag.*, **13**, 236–242.

[36] C.E. Miller, (**1985**) "Structural implications of basilar membrane compliance measurements", *J. Acoust. Soc. Am*, **77**, 1465–1474.

[37] S.T. Neely and D.O. Kim, (**1986**), "A model for active elements in cochlear biomechanics", *J. Acoust. Soc. Am.*, **79**, 1472–1480.

[38] E.S. Olson and D.C. Mountain, (**1991**, "*In vivo* measurement of basilar membrane stiffness", *J. Acoust. Soc. Am.*, **89** (3), 1262–1275.

[39] D. O'Shaughnessy (**1990**), *Speech Communication*, Addison–Wesley Pub. Co.

[40] G. Peterson, H. Barney (**1952**), "Control methods used in a study of vowels", *J. Acoust. Soc. Am.*, **24**, 175–184.

[41] J.O. Pickles, (**1988**), *An introduction to the physiology of hearing*, Academic Press.

[42] G.P. Richardson, I.J. Russell, R.Wasserkort and M. Hans, (**1989**) "Aminoglycoside antibiotics and lectins cause irreversible increases in the stiffness of cochlear hair–cell stereocilia", in *Cochlear Mechanisms. Structure, Function and Models*, J.P. Wilson and D.T. Kemp Eds., Plenum Press (New York).

[43] L. Robles, M.A. Ruggero and N.C. Rich, (**1986**), "Basilar membrane mechanics at the base of the chinchilla cochlea. I. Input–output functions, tuning curves and response phases.", *J. Acoust. Soc. Am.*, **80**, 1364–1374.

[44] M.A. Ruggero and Nola C. Rich, (**1991**), "Furosemide alters organ of Corti mechanics: evidence for feedback of outer hair cells upon the basilar membrane", *J. Neurosc.*, **11**(4), 1057–1067.

[45] H.E. Secker–Walker and C.L. Searle, (**1990**), "Time–domain analysis of auditory–nerve fibre firing rates", *J. Acoust. Soc. Am.*, **88**, 1427–1436.

[46] P.M. Sellick, R. Patuzzi and B.M. Johnston, (**1982**), "Measurement of basilar membrane motion in the guinea pig using the Moessbauer technique", *J. Acoust. Soc. Am.*, **72**, 131–141.

[47] N. Slepecky and S.C. Chamberlain, (**1987**), "Tropomyosin co–localizes with actin microfilaments and microtubules within supporting cells of the inner ear", *Cell Tissue Res.*, **248**, 63–66.

[48] H. Spoendlin, (**1978**), "The afferent innervation of the cochlea", in *Evoked Electrical Activity in the Auditory Nervous System*, (eds.) R.F. Naunton and C. Fernandez, pp. 21–39, Academic Press, London.

[49] K.P. Steel, (**1986**), "Tectorial membrane", in *Neurobiology of hearing: the cochlea* pp. 139–147, R.A. Altschuler, D.W. Hoffman and R.P. Bobbin Eds., Raven Press, New York.

[50] D.J. Tritton, (**1977**), *Physical Fluid Dynamics*, Van Nostrand Reinhold (UK) Co. Ltd.

[51] L. Voldřich (**1983**), "Experimental and topographic morphology in cochlear mechanics", in *Mechanics of Hearing*, E. de Boer and M.A. Viergever, Delft Univ. Press, Delft.

[52] E.G. Wever, (**1938**), "The width of the basilar membrane in man", *Annal. Otol. Rhinol. Laryngol.*, **48**, 38–52.

[53] J.P. Wilson, (**1980**), "Evidence for a cochlear origin for acoustic re–emission, threshold fine structure and tonal tinnitus", *Hear. Res.*, **2**, 233–252.

[54] E. Zwicker, (**1986**), "A hardware cochlear nonlinear preprocessing model with active feedback", *J. Acoust. Soc. Am.*, **80**, 146–153.